Exosomes and their miRNA cargo in retinal health and degeneration: mediators of homeostasis, and vehicles for targeted gene therapy.

Running title: Retinal exosomes mediate immune homeostasis.

Yvette Wooff[1,2†], Adrian V. Cioanca[1†], Joshua A. Chu-Tan[1,2], Riemke Aggio-Bruce[1,2], Ulrike Schumann[1], Riccardo Natoli[1,2]*.

[1] The John Curtin School of Medical Research, The Australian National University, Canberra, ACT, Australia.
[2] The ANU Medical School, The Australian National University, Canberra, ACT, Australia.

[†] Authors contributed equally

*corresponding author
Email: Riccardo.natoli@anu.edu.au

Keywords: Retina[1], neurodegeneration[2], exosome[3], microRNA[4], immuno-modulation[5], gene therapy[6].

Words: 9102

Figures: 8

Abstract:

Photoreceptor cell death and inflammation are known to occur progressively in retinal degenerative diseases, however the molecular mechanisms underlying these biological processes are largely unknown. Exosomes are essential mediators of cell-to-cell communication with emerging roles in the modulation of immune responses. Exosomes encapsulate and transfer nucleic acids, including microRNA (miRNA), to recipient cells which in disease may result in dysfunctional immune responses and a loss of homeostatic regulation. In this work we investigated the role of retinal exosomes in both the healthy and degenerating retina.

Isolated exosomes from normal retinas were characterized using dynamic light scattering, transmission electron microscopy and western blotting, and quantified across 5 days of photo-oxidative damage-induced degeneration using nanotracking analysis. Small RNAseq was used to characterize the miRNA cargo of retinal exosomes isolated from healthy and damaged retinas. Finally, the effect of exosome inhibition on cell-to-cell miRNA transfer and immune modulation was conducted using systemic daily administration of exosome inhibitor GW4869 and *in situ* hybridization of exosome-abundant miRNA, miR-124-3p. Electroretinography and immunohistochemistry was performed to assess functional and morphological changes to the retina as a result of exosome depletion.

Results demonstrated an inverse correlation between exosome secretion and photoreceptor survivability, with a decrease in exosome numbers following degeneration. Small RNAseq however revealed that there was no differential change in exosomal miRNA between groups. Inhibition of exosome biogenesis was also found to exacerbate retinal degeneration, with reduced retinal function and increased levels of inflammation and cell death demonstrated following photo-oxidative damage in exosome-depleted mice. Further, GW4869-treated mice displayed impaired translocation of photoreceptor-derived miR-124-3p to the inner retina during damage.

Taken together, we propose that retinal exosomes and their miRNA cargo play an essential role in maintaining retinal homeostasis through immune-modulation, and have the potential to be used in targeted gene therapy for retinal degenerative diseases.

1 Introduction

Retinal degenerative diseases comprise a heterogeneous group of visual disorders associated with neuroinflammation and the progressive death of retinal neurons, often resulting in irreversible blindness (Ratnapriya and Swaroop 2013). Despite advances in understanding the pathogenesis and progression of retinal degenerative diseases (Donoso, Kim et al. 2006, Janik-Papis, Ulińska et al. 2009, Knickelbein, Chan et al. 2015), the precise molecular mechanisms that propagate retinal inflammation and subsequent cell death remain unknown. The study of extracellular vesicles (EV), and in particular exosomes, might provide greater clarity in unpicking these mechanisms given their role as endogenous modulators of biological processes, including in inflammation (Chan, Wong et al. 2019), and intracellular communication pathways (Yuana, Sturk et al. 2013, L Isola and Chen 2017, Mathieu, Martin-Jaular et al. 2019).

EV are small membrane-enclosed delivery vehicles which have been widely investigated for their vital role in mediating cell-to-cell communication in both healthy as well as diseased states (Yuana, Sturk et al. 2013, L Isola and Chen 2017, Mathieu, Martin-Jaular et al. 2019). Exosomes, the smallest EV fraction (40-200nm in diameter) (Vella, Scicluna et al. 2017, Hessvik and Llorente 2018, Słomka, Urban et al. 2018), in particular, have recently been implicated in the pathogenesis of retinal degenerative diseases. These include Age-Related Macular Degeneration (AMD)(Wang, Lukas et al. 2009, Klingeborn, Dismuke et al. 2017, Hsu, Chiu et al. 2018, Li, Zhao et al. 2019), Diabetic Retinopathy (Huang, Fisher et al. 2018), and Retinitis Pigmentosa (Vidal-Gil, Sancho-Pelluz et al. 2019).

Exosomes are released by nearly all cell types and are formed via the endocytic pathway, with the invagination of the endosomal membrane allowing intraluminal vesicle formation in multivesicular bodies (MVB) (Van Niel, Porto-Carreiro et al. 2006). Biogenesis occurs either in an endosomal sorting complex required for transport (ESCRT)-dependent or ESCRT-independent manner (Kowal, Tkach et al. 2014, Li, Zhao et al. 2019), the latter of which can be blocked using GW4869, a non-competitive inhibitor of neutral sphingomyelinase 2 (nSMase2) – the key enzyme for generating exosomes via the ESCRT-independent pathway (Luberto, Hassler et al. 2002). Following biogenesis, the MVB fuses with the host cell plasma membrane and releases the internalized exosomes into the extracellular environment (Van Niel, Porto-Carreiro et al. 2006, Abels and Breakefield 2016, Hessvik and Llorente 2018). From

here, exosomes can travel to nearby or distant target cells, often through biological fluids such as blood (Charlotte, Jose et al. 2016), to exert their biological effects (Van der Pol, Böing et al. 2012, Yáñez-Mó, Siljander et al. 2015, Abels and Breakefield 2016). As exosomes selectively incorporate proteins, mRNA and non-coding RNA such as microRNA (miRNA) from their host cell (reviewed in (Yáñez-Mó, Siljander et al. 2015, Abels and Breakefield 2016)), the transfer of exosomal contents can alter the environment of target recipient cells. In a healthy state, the transfer of exosomal nucleic acid contents, including miRNA, is required for homeostatic maintenance (Desdín-Micó and Mittelbrunn 2017, Fleshner and Crane 2017). However, in disease, aberrations to this process or the selective encapsulation of toxic proteins and/or dysregulated miRNA, can cause progressive inflammation (Gupta and Pulliam 2014, Alexander, Hu et al. 2015).

MiRNA have been labelled as 'master regulators' of gene expression, due to their ability to target and repress multiple genes within and across different biological pathways (Christopher, Kaur et al. 2016). This regulatory power makes them ideal therapeutic and diagnostic molecules (Rupaimoole and Slack 2017), in particular to combat dysregulated immune responses, such as those occurring in retinal degenerations (Bartel 2009, Christopher, Kaur et al. 2016). MiRNA have been reported to be enriched in exosomes over their host cells, suggesting that they are selectively incorporated to serve a dynamic, fast-response biological need (Squadrito, Baer et al. 2014, Bhome, Del Vecchio et al. 2018).

The biological importance of exosomes and exosomal-miRNA (exoMiR) is reflected by their association with a range of inflammatory (Van Hezel, Nieuwland et al. 2017, Cypryk, Nyman et al. 2018), autoimmune (Long, Wang et al. 2018, Anel, Gallego-Lleyda et al. 2019) and neurodegenerative diseases (Jan, Malik et al. 2017, Soria, Pampliega et al. 2017, Jain, Stuendl et al. 2019). These include diabetes (Saeedi Borujeni, Esfandiary et al. 2018), rheumatoid arthritis (Skriner, Adolph et al. 2006, Zhang, Liu et al. 2006, Wan, Su et al. 2019), and Alzheimer's and Parkinson's disease (Gupta and Pulliam 2014, Li, Wang et al. 2018, Jain, Stuendl et al. 2019, Sackmann, Sardar Sinha et al. 2019). ExoMiR have been reported to play pathogenic roles in these diseases by promoting angiogenesis (Kosaka, Iguchi et al. 2013, Atienzar-Aroca, Flores-Bellver et al. 2016),-and modulating immune responses, including in the recruitment of immune cells (Théry, Zitvogel et al. 2002, Abusamra, Zhong et al. 2005, Robbins and Morelli 2014, Ye, Li et al. 2014, Wong, Lee et al. 2016, Van Hezel, Nieuwland et al. 2017); features that contribute to cell death. To date however, the identification and role

of exosomes and their miRNA cargo in the retina in both healthy and diseased states, is largely unexplored (Klingeborn, Dismuke et al. 2017, Li, Zhao et al. 2019).

Characterizing the role of exosomes and their miRNA cargo in both the normal and degenerating retina will aid in elucidating novel cell-to-cell communication pathways that could play a role in propagating inflammation during retinal degenerative diseases. Furthermore, uncovering the miRNA signature within retinal exosomes as well as their potential binding partners may reveal novel regulatory mechanisms underpinning retinal degenerations, ultimately leading to the discovery of therapeutic targets. This study characterizes for the first time, retinal-derived exosomes from both the healthy and degenerating mouse retina.

We show that exosome secretion is inversely correlated to photoreceptor survivability, with the severity of retinal degeneration directly correlating to decreased retinal exosomes numbers. We used small RNAseq to characterize the miRNA cargo of retinal exosomes (exoMiR). Although we demonstrated that there was no change in exosome miRNA-cargo in response to retinal degeneration, we found that the top 10 exoMiR contained in retinal exosomes were associated with the regulation of inflammatory, cell survival and motility pathways. Upon systemic exosome inhibition using GW4869, retinal function in healthy and photo-oxidative damaged mice was significantly reduced compared to controls. In addition, photoreceptor cell death and inflammation were significantly increased in GW4869-injected photo-oxidative damaged mice, compared to controls. Using *in situ* hybridization, we further demonstrated that the transport of miR-124-3p from the outer to inner retina was impaired in GW4869-injected photo-oxidative damaged mice, suggesting that miR-124-3p movement is exosome-dependent.

Taken together, these results suggest a novel role for exosomes and exoMiR-mediated cell-to-cell communication in the retina. We demonstrate that maintaining and transporting necessary levels of exosome cargo is required for normal retinal homeostasis and immunomodulation, with insufficient bioavailability of exosomes potentially leading to inflammatory cell death (see Figure 8). In addition, this work elucidates downstream biological targets of exoMiR that are required for retinal homeostatic maintenance, and identifies potential miRNA and mRNA therapeutic targets for further investigations.

2 Materials and Methods

2.1 Animal handling and photo-oxidative damage

All experiments were conducted in accordance with the ARVO Statement for the Use of Animals in Ophthalmic and Vision Research and with approval from the Australian National University's (ANU) Animal Experimentation Ethics Committee (AEEC) (Ethics ID: A2017/41; Rodent models and treatments for retinal degenerations). Adult male and female C57BL/6J wild-type (WT) mice (aged between 50-90 postnatal days) were bred and reared under 12 h light/dark cycle conditions (5 lux) with free access to food and water. The C57BL/6J colony was genotyped for the presence of both the $Rpe65^{450Met}$ polymorphism or the deleterious $Crb1^{rd8}$ mutation using previously published primer sets (Kim, Fishkin et al. 2004, Mattapallil, Wawrousek et al. 2012). Sequencing for these was conducted at the ACRF Biomolecular Resource Facility, ANU. All animals used possessed the $Rpe65^{450Met}$ polymorphism but were free of the $Crb1^{rd8}$ mutation. Littermate age-matched WT mice were randomly assigned to photo-oxidative damage (PD) and dim-reared control (DR) groups. Animals in the photo-oxidative damage group were continuously exposed to 100K lux white LED light for a period of 1, 3, or 5 days as described previously (Natoli, Jiao et al. 2016), with the majority of experiments conducted for 5 days. Dim-reared mice were maintained in 12h light (5 lux)/dark cycle conditions.

2.2 Retinal exosome isolation

Mice were euthanized with CO_2 following experimental runs. Either two (from one mouse) or four (from two mice - used for high-throughput sequencing) retinas were pooled and collected in Hanks Buffered Saline Solution (HBSS, Gibco; Thermo Fisher Scientific, MA, USA). Retinas were transferred to 500µL digestion solution ((HBSS containing 2.5mg/mL papain (Worthington Biochemical, NJ, USA), 200U DNase I (Roche Diagnostics, NSW, AUS), 5µg/mL catalase (Sigma-Aldrich, MO, USA), 10µg/mL gentamycin (Sigma-Aldrich, MO, USA) and 5µg/mL superoxide dismutase (Worthington Biochemical, NJ, USA)) and finely chopped using scissors. Retinas were incubated at 37°C for 8 minutes, followed by 20 minutes at 8°C, to allow for the breakdown of the extracellular matrix and exosome release. Following digestion, tissue suspensions were neutralized by diluting in 11.5mL of HBSS and centrifuged at 1000xg for 10 minutes at 4°C to remove cells and cell debris. The supernatant was transferred to 14x89mm Beckman Ultra-Clear ultracentrifuge tubes (Beckman Coulter,

CA USA) and centrifuged at 10,000xg for 30 minutes at 4°C in a Beckman Coulter Optima XE-100 (fitted with a SW41Ti Rotor (Beckman Coulter, CA USA)), to collect microvesicles and remaining cell debris. The exosome-containing supernatant was transferred to new ultracentrifuge tubes and centrifuged for 1.5 hours at 150,000xg at 4°C. The supernatant was carefully decanted, and the exosome pellet resuspended via tituration for 1 minute in 500µL Ultrapure Endotoxin-free 0.1M PBS (Thermo Fisher Scientific, MA, USA) and used immediately for quantification.

For RNA isolation, the exosome pellet was resuspended immediately in 100µl RNAse A (10µg/ml in Ultrapure Endotoxin-free 0.1M PBS) and incubated for 30 minutes at 37°C to digest any RNA contamination. Following RNase treatment, exosomal RNA was extracted using the mirVana miRNA Isolation Kit (Thermo Fisher Scientific, MA, USA) as per section 2.8.

2.3 Exosome Characterization

2.3.1 NanoSight

The size and concentration of exosomes were measured using nanoparticle tracking analysis on a NanoSight NS300 (Malvern Instruments, Malvern, UK). Exosome samples were diluted 1:20 (retinal exosomes) or 1:40 (cell culture exosomes) in 1ml Ultrapure Endotoxin-free 0.1M PBS to achieve a particle per frame value between 20 and 100. Samples were analyzed under constant flow provided by a syringe pump set at a speed of 35 (equating to ~3.1µl/min; (Gerritzen, Martens et al. 2017). A total of nine 30s long videos were captured (camera setting: 14) for each sample. The detection threshold was set between 4-5 and was not altered between measurements of the same experiment. The concentration values, modal and mean sizes were exported to Prism V7 (GraphPad Software, CA, USA) for statistical analysis and plotting.

2.3.2 Zetasizer

Dynamic light scattering measurements were performed using a Zetasizer Nano ZS 90 (Malvern Instruments, Malvern, UK). A 500µL undiluted retinal exosome suspension in Ultrapure Endotoxin-free 0.1M PBS was prepared, loaded in a low-volume disposable sizing cuvette (ZEN0112, Malvern Instruments, Malvern, UK) and agitated before measurements.

Measurement parameters were set as follows: Material Refractive Index – 1.46, Dispersant Refractive Index – 1.330, Viscosity (cP) – 0.888, Temperature (°C) – 25, and Measurement Duration (s) – 60. The acquired intensity data was transformed using the General-Purpose Model within the Zetasizer analysis software to generate the size distribution of the exosomes.

2.3.3 Transmission Electron Microscopy (TEM)

A 30µl retinal exosome suspension was placed on a 200-mesh carbon-coated copper grid (Sigma-Aldrich, MO USA) and pre-treated with glow discharge using an Emtech K100X system (Quorum Technologies, Sussex, UK). After 20 minutes, exosomes were contrasted with 2% uranyl acetate solution for 1 minute, followed by 3 washes in 0.22µm filtered PBS (Thermo Fisher Scientific, MA, USA). Excess PBS was removed by placing a piece of absorbent paper at the edge of the grid. The grids were imaged on a Hitachi 7100 FA transmission electron microscope (Hitachi, Tokyo, Japan) at 100kV. The images were captured with a side mounted Gatan Orius CCD camera (Gatan, CA, USA) at 4008x2672 pixels resolution using a 2 seconds exposure operated through Gatan Microscopy Suite (Gatan, CA, USA). A total of 20 images were captured at 100,000x magnification from four different grids, each containing exosomes isolated from a different retinal exosome preparation (2 mouse retinas/preparation). The images were imported into ImageJ V2.0 software (National Institutes of Health, Bethesda, MD, USA), scale-calibrated and the diameter of approximately 230 exosomes was measured. The size distribution was plotted in a histogram with 20nm wide bins using Prism V7.0 (GraphPad Software, CA, USA).

2.3.4 Western blot

Exosome pellets (see section 2.2) were immediately lysed in 50µL CellLyticTM Cell Lysis Buffer (supplemented with 1:100 protease inhibitor cocktail; Sigma-Aldrich, MO, USA). The blot was performed as previously described (Jiao, Rutar et al. 2018). Briefly,10µg of denatured protein was loaded onto Novex 4-20% Tris-Glycine Mini Gels (Thermo Fisher Scientific, MA, USA) and subjected to electrophoresis (45 minutes, 150V). The protein bands were transferred (45 minutes, 20V) to a nitrocellulose membrane (Bio-Rad, CA, USA) using the Power Blotter semi-dry system (Thermo Fisher Scientific, MA, USA). Membranes were then washed in PBS-Tween (0.025%; PBS-T), blocked in 3% BSA for 1 hour and then incubated overnight at 4°C with primary exosome marker antibodies CD63, (1:1000, Ts63, Thermo Fisher Scientific, MA, USA), CD81 (1:2000, ab109201, Abcam, Cambridge, UK) or CD9 (1:2000, ab92726, Abcam, Cambridge, UK). Following three washes in PBS-T, blots

were incubated in appropriate secondary antibodies, HRP-conjugated Goat Anti-Rabbit IgG (H+L) (1:1000, 170-6515, Bio-Rad, CA, USA) or Goat-anti-Mouse IgG (1:1000, 170-6516, Bio-Rad, CA, USA) for 2 hours at room temperature. Membranes were washed in PBS-T and developed for 2 minutes with ClarityTM Western ECL Substrate (Bio-Rad, CA, USA). Imaging was performed using a ChemiDocTM MP Imaging System with Image Lab™ software (Bio-Rad, CA, USA).

2.4 Exosome biogenesis inhibition

Exosome biogenesis inhibition was performed using GW4869 (Sigma-Aldrich, MO, USA). GW4869 was reconstituted in dimethyl sulfoxide (DMSO; Sigma-Aldrich, MO, USA) to a concentration of 5mM and used as a stock solution for further dilution in Ultrapure Endotoxin-free 0.1M PBS. Mice were injected with 1.25mg/kg GW4869 via intraperitoneal (I.P.) injection daily for 5 days. 10.3% DMSO in Ultrapure Endotoxin-free 0.1M PBS (corresponding to the final volume of DMSO in GW4869 preparations) was used as a negative control. All mice were monitored daily for signs of distress or sickness.

2.5 Retinal Assessment

2.5.1 Retinal Function via Electroretinography (ERG)

To assess retinal function full-field scotopic ERG was performed as previously described (Natoli, Fernando et al. 2017). Briefly, mice were dark-adapted overnight before being anaesthetized with an intraperitoneal injection of Ketamine (100 mg/kg; Troy Laboratories, NSW, Australia) and Xylazil (10 mg/kg; Troy Laboratories, NSW, Australia). Both pupils were dilated with one drop each of 2.5% w/v Phenylephrine hydrochloride and 1% w/v Tropicamide (Bausch and Lomb, NY, USA).

Anaesthetized and pupil dilated mice were placed on the thermally regulated stage of the Celeris ERG system (Diagnosys LLC, MA, USA). The Celeris ERG system has combined Ag/AgCl electrode-stimulator eye probes which measure the response from both eyes simultaneously, and uses 32-bit ultra-low noise amplifiers fitted with impedance testing. Eye probes were cleaned with 70% ethanol and then a 0.3% Hypromellose eye drop solution (GenTeal; Novartis, NSW, AUS) was applied to both probes. The probes were then placed

covering and just touching the surface of each eye. A single- or twin-flash paradigm was used to elicit a mixed response from rods and cones. Flash stimuli for mixed responses were provided using 6500K white flash luminance range over stimulus intensities from -0.01 - 40 log cd s m^{-2}. Responses were recorded and analyzed using Espion V6 Software (Diagnosys LLC, MA, USA). Statistics were performed in Prism V7.0 using a two-way analysis of variance (ANOVA) to test for differences in a-wave and b-wave responses. Data was expressed as the mean wave amplitude ± SEM (μV).

2.5.2 Optical Coherence Tomography (OCT)

Cross-sectional images of live mouse retinas were taken at 1mm increments from the optic nerve using a Spectralis HRA+OCT device (Heidelberg Engineering, Heidelberg, Germany) as previously described (Natoli, Jiao et al. 2016). Eye gel (GenTeal; Novartis, NSW, AUS) was administered to both eyes for recovery.

Using OCT cross-sectional retinal images, and ImageJ V2.0 software (National Institutes of Health, Bethesda, MD, USA), the thickness of the outer nuclear layer (ONL), was calculated as the ratio to the whole retinal thickness (outer limiting membrane to the inner limiting membrane). To quantify photoreceptor survival, the thickness of the ONL on retinal cryosections was determined by counting the number of nuclei rows (photoreceptor cell bodies) in the area of retinal lesion development (1mm superior to the optic nerve head). Photoreceptor cell row quantification was performed five times per retina using two retinal cryosections at comparable locations per mouse. The thickness of retinal layers, as the ratio to whole retinal thickness, was also measured in the ONL, inner nuclear layer (INL), and ganglion cell layer (GCL) in retinal cryosections.

2.6 Retinal tissue collection and preparation

Animals were euthanized with CO_2 following functional ERG analysis. The superior surface of the left eye was marked and enucleated, then immersed in 4% paraformaldehyde for 3 hours. Eyes were then cryopreserved in 15% sucrose solution overnight, embedded in OCT medium (Tissue Tek, Sakura, Japan) and cryosectioned at 12μm in a parasagittal plane (superior to inferior) using a CM 1850 Cryostat (Leica Biosystems, Germany). To ensure accurate comparisons were made for histological analysis, only sections containing the optic nerve head were used for analysis. The retina from the right eye was excised through a corneal

incision and placed into RNAlater solution (Thermo Fisher Scientific, MA, USA) at 4□C overnight and then stored at -80□C until further use.

2.7 Immunolabelling

Immunohistochemical analysis of retinal cryosections was performed as previously described (Rutar, Natoli et al. 2015). Fluorescence was visualized and images taken using a laser-scanning A1$^+$ confocal microscope at 20x magnification (Nikon, Tokyo, Japan). Images panels were analyzed using ImageJ V2.0 software and assembled using Photoshop CS6 software (Adobe Systems, CA, USA).

2.7.1 IBA-1 Immunohistochemistry

Immunolabeling for IBA-1 (1:500, 019-19741, Wako, Osaka, Japan) and quantification was performed as previously described (Rutar, Natoli et al. 2015). The number of IBA-1$^+$ cells (a marker of retinal microglia and macrophages) was counted across the superior and inferior retina using two retinal sections per mouse and then averaged. Retinal cryosections were stained with the DNA-specific dye bisbenzimide (1:10000, Sigma-Aldrich, MO, USA) to visualize the cellular layers.

2.7.2 TUNEL assay

Terminal deoxynucleotidyl transferase (Tdt) dUTP nick end labelling (TUNEL), was used as a measure of photoreceptor cell death. TUNEL *in situ* labelling was performed on retinal cryosections using a Tdt enzyme (Cat# 3333566001, Sigma-Aldrich, MO, USA) and biotinylated deoxyuridine triphosphate (dUTP) (Cat# 11093070910, Sigma-Aldrich, MO, USA) as previously described (Natoli, Zhu et al. 2010). Images of TUNEL staining were captured with the A1$^+$ Nikon confocal microscope at 20x magnification. The total number of TUNEL$^+$ cells were counted including both the superior and inferior retina using two retinal sections per animal, and is represented as the average number of TUNEL$^+$ cells per retinal section.

2.7.3 *In situ* hybridization

Localization of miR-124-3p within the retina was determined by *in situ* hybridization. A double DIG-labelled miR-124-3p miRCURY LNA miRNA Detection Probe (Exiqon, Vedbaek, Denmark) was used on retinal cryosections, which were hybridized for 1 hour at 53°C as previously described (Chu-Tan, Rutar et al. 2018). The bound probe was visualized

using 5-bromo-4-chloro-3 indoyl phosphate (NBT/BCIP; Sigma-Aldrich Corp., St. Louis, MO, USA). Bright field images were captured on the A1^{+} Nikon confocal microscope fitted with a DS-Ri1-U3 color camera at 20x magnification and 4076x3116 pixel resolution. All images were centered at the site of lesion located approximately 1mm superiorly to the optic nerve head. The images were imported into ImageJ V2.0 software, converted to 8-bit format and then the mean grey values were measured at five different locations along the INL, ONL and the outer limiting membrane/photoreceptor inner segment region.

2.8 RNA extraction

RNA (enriched for miRNA) extraction and purification from retinas or RNase A treated exosome pellets was performed using an acid-phenol:chloroform extraction method with the mirVana miRNA Isolation Kit (Thermo Fisher Scientific, MA, USA) according to the manufacturer's instructions. The concentration and purity of each RNA sample was assessed using the ND-1000 spectrophotometer (Nanodrop Technologies, DE, USA). The size distribution and concentration of exosomal miRNA was further assessed using a 2100 Agilent Bioanalyzer with an Agilent Small RNA Kit (Agilent Technologies, CA, USA), according to the manufacturers' instruction.

2.8.1 cDNA synthesis from mRNA templates

Following purification of RNA, cDNA was synthesized from 1µg RNA using Tetro cDNA Synthesis Kit (Bioline Reagents, London, UK), according to manufacturer's instructions.

2.8.2 Quantitative real-time polymerase chain reaction:

Gene expression was measured by qRT-PCR using mouse specific TaqMan hydrolysis probes (Table 1) and TaqMan Gene Expression Master Mix (Thermo Fisher Scientific, MA, USA). Reactions were performed in technical duplicates in a 384-well format using a QuantStudio 12 K Flex RT-PCR machine (Thermo Fisher Scientific, MA, USA). Data was analyzed using the comparative C_t method ($\Delta\Delta C_t$) and results are presented as percent change relative to control. Expression was normalized to reference gene glyceraldehyde-3-phosphate dehydrogenase (*Gapdh*).

Table 1: TaqMan Hydrolysis probes (Thermo Fisher Scientific, MA, USA) used for qPCR.

Gene symbols	Gene name	Catalogue number
Pdcd6ip	Programmed Cell Death 6 Interacting Domain	Mm00478032_m1
Smpd3	Sphingomyelin Phosphodiesterase 3	Mm00491359_m1
Gapdh	Glyceraldehyde-3-Phosphatase Dehydrogenase	Mm01536933_m1

2.9 Small RNA high-throughput sequencing

2.9.1 Library preparation and sequencing

cDNA libraries from miRNA-enriched exosome RNA samples were prepared by the John Curtin School of Medical Research Biomolecular Research Facility (JCSMR, BRF, ACT, AUS), using the Capture and Amplification by Tailing and Switching method (CATS RNA-seq Kit v2 x24, Diagenode Cat# C05010041, Leige, Belgium). 10ng RNA was used as input and the dephosphorylation step omitted to select for 3'-OH RNA species (miRNA). The library was amplified with 9 PCR cycles and cleaned with 0.9x AMPure® XP beads (A63881, Beckman Coulter, CA, USA) to enrich for DNA fragments shorter than 50nt. Libraries were multiplexed and sequenced on a single lane using the Illumina NextSeq500 (Illumina, CA, USA) acquiring 50 base-pairs single-end reads. The sequencing depth was between 8 and 15 million reads/sample with an average phred read quality of 33 (Figure S3 A).

2.9.2 Bioinformatics

Sequencing reads were initially checked for quality scores, adapter/index content and K-mer content using FastQC v0.11.8 (Babraham Bioinformatics, Cambridge, UK), then imported into Partek® Flow® (Partek Inc, MO, USA) for all subsequent analyses. Base composition analysis indicated the presence of an enriched poly-A tail and the CATS template-switching nucleotide within the first 3 base-pairs of the reads (Figure S3 B), indicating a successful library preparation. A trimming pipeline was created according to the following cutadapt code "cutadapt --trim-n -a GATCGGAAGAGCACACGTCTG -a AGAGCACACGTCTG

<input.file> | cutadapt -u 3 -a AAAAAAAAAACAAAAAAAAAA -e 0.16666666666666666 - | cutadapt -g GTTCAGAGTTCTACAGTCCGACGATC -m 18 -o <output.file> -", to remove the template switching nucleotide and the 3' and 5' adapters associated with the CATS library preparation. After trimming, the base composition was centered around 25% for each nucleotide (Figure S3 C), and FastQC analysis confirmed the effective removal of the 3' and 5' adapters and indices.

Trimmed reads were aligned against the mature mouse miRNA downloaded from miRbase v.22 using the Burrows-Wheeler Aligner (BWA) in backtrack mode with parameters -n 1(base), -o 1, -e -1, -d 10, -i 5, -k 2, -E 4, -R 30, -t 24 (as recommended by (Ziemann, Kaspi et al. 2016). MiRNAs with less than 10 alignments across all samples were discarded from the subsequent analyses. Reads aligned to miRbase v.22 (mature miRNAs) with BWA had a length distribution between 18-24 nucleotides consistent with the expected length of mature miRNA (Figure S3 D). Aligned reads were normalized using the Trimmed means of M (TMM) and Upper Quartile (UQ) methods as recommended (Tam, Tsao et al. 2015), with the latter being chosen as the preferred method as it produced less variable means and distributions (Figure S3, E, F and G). After normalization, a two-dimensional principal component analysis was performed in Partek® Flow® (Partek Inc, MO, USA) to assess the clustering of the samples and identify outliers. Fold changes and statistical significance were computed using the Gene Specific Analysis (GSA) tool within Partek® Flow® (Partek Inc, MO, USA). This function uses the corrected Akaike Information Criterion to select the best statistical model for each gene from the available Normal, Negative Binomial, Lognormal or Lognormal with shrinkage options. Lognormal with shrinkage (Wu, Wang et al. 2013), produced the best fit and thus was selected to perform differential analysis. A dataset was created containing the expression values for each miRNA in all samples and imported into R (Team 2019). The counts were log2 transformed to display the distribution of miRNAs in dim-reared and photo-oxidative samples using the packages ggbeeswarm (Erik Clarke 2017) and ggplot2 (Wickham 2016). Hierarchical clustering analysis (HCA) was performed in Partek® Flow® (Partek Inc, MO, USA) using the Euclidian distance as a point metric distance and the average linkage as the agglomerative method.Sequencing data can be accessed from BioProject (Accession ID: PRJNA615966).

2.9.3 Network and pathway enrichment analysis

The miRNet platform (Fan, Siklenka et al. 2016) was used to elucidate potential interactions between exosomal miRNA and retinal mRNA. The mRNA dataset is available from BioProject (accession ID: PRJNA606092) and comprises of all retinal genes with a $\log_2$(count per million) value > -2.4 (Table S2). The retinal targetome of the top 10 exosomal miRNAs was imported into Enrichr (Chen, Tan et al. 2013) and analyzed for over-expressed pathways annotated in Wikipathways (Slenter, Kutmon et al. 2018) (mouse annotation), and gene-disease associations listed in DisGeNet database (Piñero, Bravo et al. 2016).

2.10 *In vitro* experiments

2.10.1 661W cell culture

Murine photoreceptor-derived 661W cells (kindly gifted by Dr. Muayyad R. Al-Ubaidi, Dept. of Biomedical Engineering, University of Houston, Houston, TX, USA) (Al-Ubaidi, Hollyfield et al. 1992), were used for *in vitro* experiments at passage 1-5. The authenticity of the of the cells was validated by short tandem repeat analysis (CellBank, Sydney, AUS). Cells were cultured in growth media (Dulbecco's Modified Eagle Medium (DMEM; Sigma-Aldrich, MO, USA) supplemented with 10% fetal bovine serum (FBS; Sigma-Aldrich, MO, USA), 6 mM L-glutamine (Thermo Fisher Scientific, MA, USA) and antibiotic-antimycotic (100U/ml penicillin, 100 µg/ml streptomycin; Thermo Fisher Scientific, MA, USA)), as previously published (Lu, Fernando et al. 2018). Cells were maintained and all incubation steps were performed in dark conditions in a humidified atmosphere of 5% CO_2 at 37°C, unless otherwise stated. Cells were passaged by trypsinization every 3 – 4 days.

2.10.2 *In vitro* photo-oxidative damage

661W cells were seeded in 96 well plates (Nunc, Thermo Fisher Scientific, MA, USA) at $2x10^5$ cells/well 24 hours prior to photo-oxidative damage experiments. Cells were exposed for 5 hours to 15,000 lux light (2.2 mW/cm^2; irradiance measured with PM100D optical power meter, THORLABS, NJ, USA) from two white fluorescent lamps (2 × 10W T4 tri-phosphor 6500K daylight fluorescent tubes; Crompton, NSW, Australia). Control cells were completely wrapped in aluminum foil with six small incisions to allow air/gas exchange.

For exosome inhibition experiments, both 661W cells undergoing photo-oxidative damage or grown under dim conditions were treated with GW4869 at 5, 20 and 40µM diluted from

stock solution, in DMEM supplemented with 1% FBS, 6mM L-glutamine and antibiotic-antimycotic (100U/ml penicillin, 100 µg/ml streptomycin), while control dim and photo-oxidative damage wells were treated with equivalent concentrations of DMSO.

2.10.3 Cell viability by MTT assay

Cell viability was tested by 3-(4,5-dimethylthiazol-2-yl)-2,5-diphenyltetrazolium bromide (MTT) assay (Roche, Mannheim, Germany), according to manufacturer's instructions. Briefly, conditioned media was discarded and 100µl growth media containing 10% MTT was added to all wells. The cells were incubated for 4 hours to allow for the formation of formazan crystals. The 100µl of solubilization buffer was added to each well and cells incubated for 18 hours. The absorbance at 570nm of each well was measured with a 670nm reference wavelength using an Infinite® 200 Pro plate reader (Tecan, Mannedorf, Switzerland). Background absorbance (wells containing medium with MTT reagent only) was subtracted from all sample wells and the viability calculated by dividing the absorbance of treated wells (DMSO or GW4869) by controls (cell treated with medium only).

2.10.4 Exosome inhibition in 661W cells

To deplete FBS of exosomes, the serum was centrifuged (200,000xg, at 4°C for 18 hours) using a Beckman Coulter Optima XE-100 Ultracentrifuge (Beckman Coulter, CA, USA), with a SW41Ti rotor (Beckman Coulter, CA USA) and the supernatant used as FBS supplement in all GW4869 experiments (adjusted growth media).

To test the effect of GW4869 on inhibiting exosome biogenesis, 661W cells were seeded at a density of $1x10^5$ cells/well in 6 well plates (Nunc, Thermo Fisher Scientific, MA, USA) and grown to 80% confluence in growth medium. Media was removed and cells treated with 20µM GW4869, or equivalent DMSO, in adjusted growth media for 4h. The conditioned medium from four GW4869-treated or control wells was pooled and processed for exosome isolation and characterization as described in Sections 2.2 and 2.3.1.

2.11 Statistical analyses:

All graphing and statistical analyses were performed using Prism V7.0, unless otherwise specified. An unpaired Student's *t*-test, one-way analysis of variance (ANOVA), or two-way ANOVA with Tukey's multiple comparison post-hoc test was utilized as appropriate to determine the statistical outcome. Non-adjusted p values ($P<0.05$) or false-discovery adjusted

p values (FDR<0.1) were deemed statistically significant. All data was expressed as the mean ± SEM.

3 Results

3.1 Retinal exosome isolation

To date, the isolation of retinal exosomes has not been reported. Using a modified dissociation protocol (Figure 1A) (Rutar, Natoli et al. 2015), retinas from 2 mice were pooled together, digested with papain to produce a single cell suspension (S1) from which retinal extracellular vesicles could be secreted, and resuspended in a large volume of HBSS. Following, S1 was centrifuged at 1000xg to remove cells and cellular debris, termed pellet 1 (P1). The supernatant (S2) was subsequently centrifuged at 10,000xg to remove the microvesicle EV fraction (P2), and the remaining supernatant (S3) centrifuged again at 150,000xg to isolate exosomes (P3). P3 was either resuspended in HBSS for exosome quantification, or subjected to RNase treatment prior to RNA extraction (Figure 1A). Extracellular vesicles isolated from dim-reared retinas displayed exosomal properties, including the distinctive round, cup-shaped morphology (Jung and Mun 2018) as seen in representative negative-stained TEM images (Figure 1B, and Figure S1A). Isolated vesicles were within the expected size-range of exosomes (40-200nm; (Théry, Zitvogel et al. 2002, Hessvik and Llorente 2018, Słomka, Urban et al. 2018), as shown by TEM size distribution histogram, nanotracking analysis using NanoSight NS300 and dynamic light scatter using a Zetasizer Nano instrument (Figure 1C-F). Further, isolated vesicles displayed known exosome markers CD63, CD81 and CD9, as determined by western blotting (Figure 1G).

Exosome Isolation Method Summary

A Experimental workflow

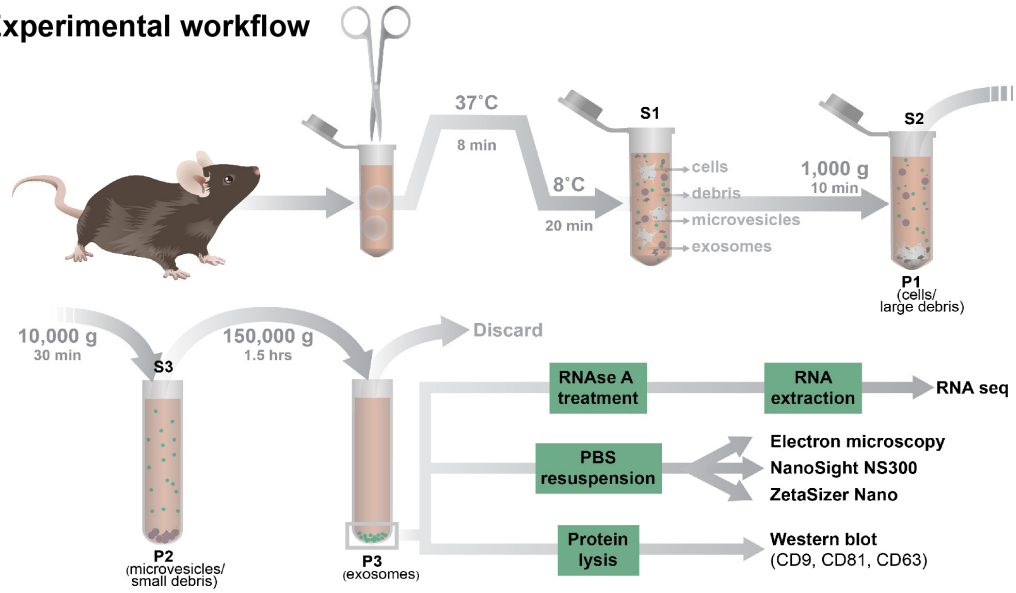

Exosome Characterisation

B Representative TEM

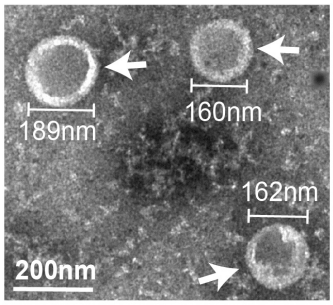

C Size distribution (TEM)

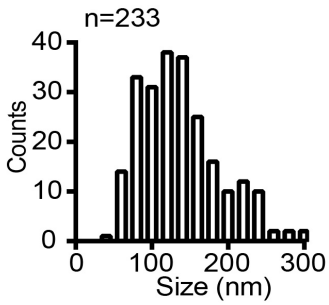

D Size distribution (NanoSight)

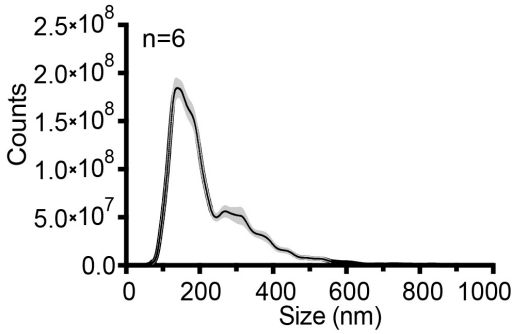

E NanoSight data statistics

Retinas/ sample	# of samples	Concentration ($x10^{10}$ vesicles/ml)	Mean size (nm)	Modal Size (nm)
4	6	3.81 ± 1.06	189 ± 16.9	156 ± 16.6

F Size distribution (DLS Zetasizer)

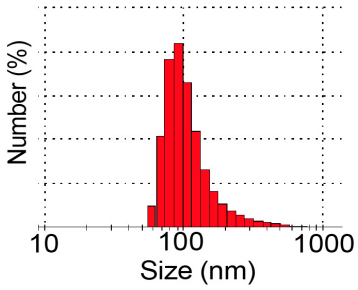

G Expression of exosome markers

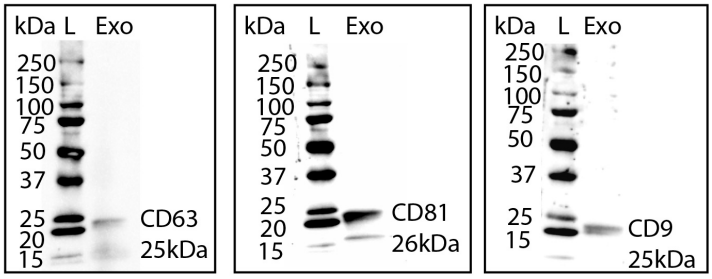

Figure 1: Retinal exosome isolation and characterization

(A) Workflow for the isolation and characterization of retinal exosomes. Exosomes were isolated from papain-digested retinas using differential ultracentrifugation. Exosome pellets (P3) were processed for RNA extraction and RNA sequencing (RNA seq) and size and morphology analysis by electron microscopy, NanoSight NS300 and Zetasizer Nano. Exosome pellets were also digested in protein lysis buffer and analyzed for the expression of exosome markers CD9, CD81 and CD63 by western blot. S=supernatant, P=pellet. **(B)** Representative Transmission Electron Microscopy (TEM) micrograph showing isolated retinal vesicles (white arrows) with consistent round, cup-shaped morphology and size of exosomes. **(C)** Diameter distribution of retinal exosomes measured from TEM micrographs (n=233). **(D)** Size distribution of retinal exosomes (n=6 samples, 4 retinas/sample) using nanotracking analysis performed on a NanoSight NS300. **(E)** Average concentration, mean and modal size of exosomes isolated from mouse retinas measured by nanotracking analysis (n=6 samples, 4 retinas/sample). **(F)** Representative plot of the size distribution of exosomes measured by dynamic light scatter (DLS) using a Zetasizer Nano instrument (n=5). **(G)** Full-length western blots showing the presence of exosomal markers CD63 (25kDa), CD9 (26kDa) and CD81 (25kDa) in retinal exosome protein lysates (Exo). Molecular weight standard (L).

3.2 Retinal exosomes decrease in concentration but not size, during photo-oxidative damage-induced degeneration.

Following the characterization of retinal exosomes isolated from dim-reared retinas, the effect of photo-oxidative damage on the secretion of exosomes was investigated. The relative retinal exosome concentration was found to decrease in a damage-dependent manner, reducing significantly from dim-reared controls by 17±2.7% after up to 3 days of photo-oxidative damage and 38 +/- 4.0% after 5 days of photo-oxidative damage (Figure 2A). While the exosome concentration after 5 days of photo-oxidative damage was decreased from (4.27±0.2) $x10^{10}$ vesicles/ml to (2.82±-0.3) $x10^{10}$ vesicles/ml (Figure 2B). The analysis of the size distribution of exosomes at these two timepoints showed that vesicles with diameter of up to 200nm had a more pronounced decrease in numbers (Figure 3C). The mean and modal size of exosomes remained unchanged after 5 days of photo-oxidative damage (Figure 2D). Taken together these results suggest that while there is no change in the size of isolated exosomes, there was a progressive reduction in the concentration of exosomes during photo-oxidative damage-induced degeneration. These results correlate with an increased level of photoreceptor cell death and increased retinal inflammation that occurs during photo-oxidative damage (Natoli, Jiao et al. 2016).

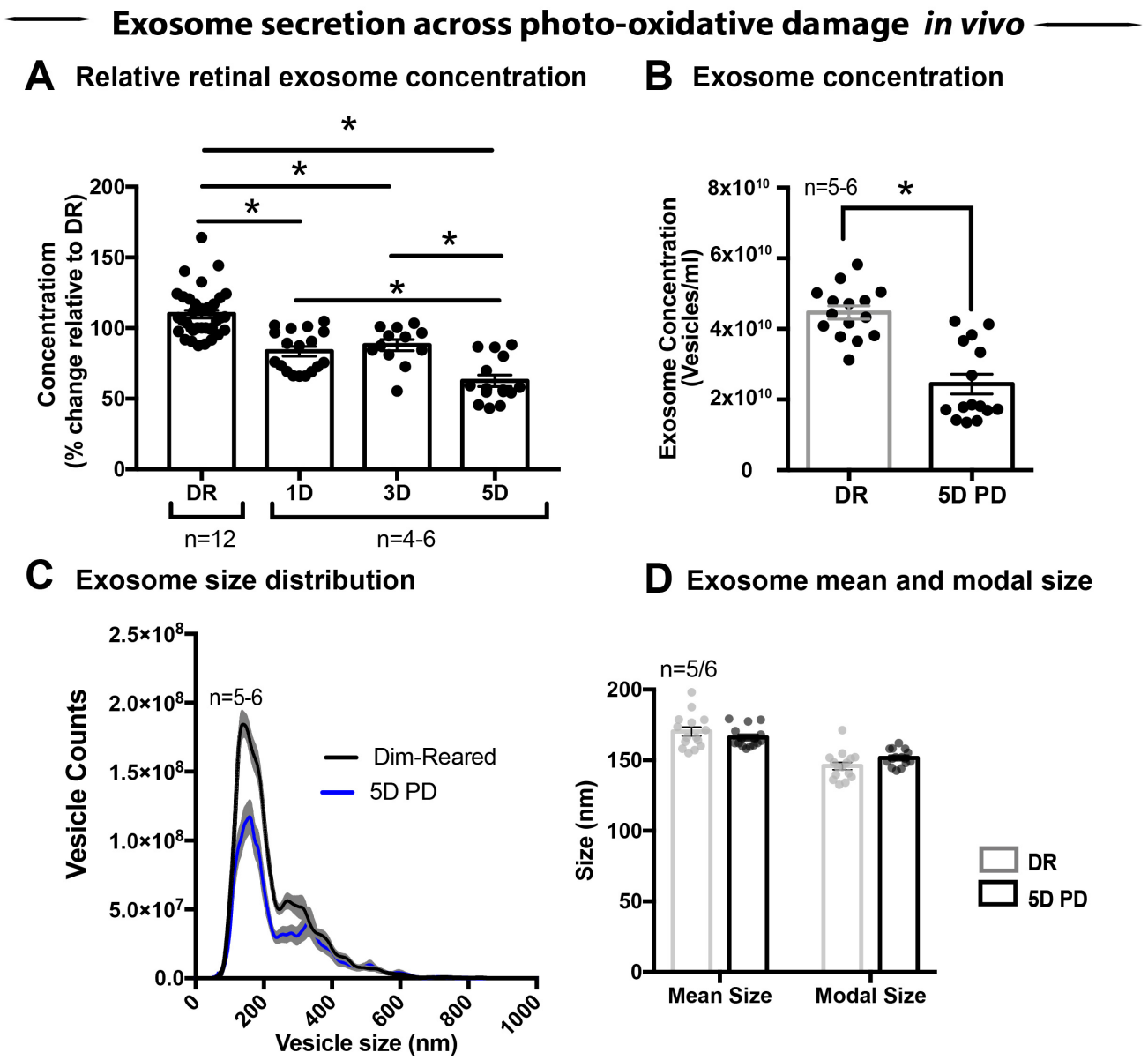

Figure 2: Retinal exosomes decrease in concentration but not size, over photo-oxidative damage-induced degeneration.

(A) Concentration of retinal exosomes decreased progressively across time in PD, with significantly reduced exosomes at 1D, 3D and 5D PD compared to DR controls ($P<0.05$, n=3-12). Concentration values are presented as percentage of DR. **(B)** Significant reduction in the concentration of exosomes from 5D PD retinas compared to DR controls ($P<0.05$, n=5-6). **(C)** No significant change in the size distribution of exosomes isolated from 5D PD retinas compared to DR controls, however vesicles with size < 200nm show a marked decrease in concentration following 5D PD ($P>0.05$, n=5-6). **(D)** No difference in either the mean or modal size of retinal exosomes between DR and 5D PD groups ($P>0.05$, n=5-6). All results obtained using nanotracking analysis (NanoSight NS300).

3.3 GW4869 inhibits biogenesis of retinal exosomes.

Given the correlation between increased photoreceptor cell death and reduced retinal exosome concentration during photo-oxidative damage, the effect of exosome biogenesis inhibition on the retina was investigated using GW4869, an inhibitor of nSMase2 (Kosaka 2010). To determine efficiency, GW4869 was added in culture to 661W photoreceptor-like cells. Exosomes isolated from 661W were characterized using TEM (Figure S1B). Compared to DMSO controls, 661W exosome concentration (Figure 3A-B) was significantly reduced in GW4869-treated cells, demonstrating a high level of efficacy of this inhibitor. Furthermore, increased GW4869 concentrations did not affect cell viability compared to DMSO controls under dim conditions. However, following photo-oxidative damage (4 hours of 15,000k lux white light), an inverse dose-dependent correlation was observed between GW4869 concentration and cell viability (Figure 3C-D).

When investigated *in vivo*, exosomal isolates from the retina of GW4869-treated mice (daily IP injections for 5 days) were reduced in concentration compared to those from DMSO-injected controls. This was seen in both dim-reared and photo-oxidative damaged retinas (Figure 3E). Additionally, the expression of genes associated with ESCRT-dependent and ESCRT-independent exosome biogenesis pathways were measured by qRT-PCR. We targeted *Pdcd6ip* (also known as *Alix*), which encodes an accessory protein in the ESCRT-dependent pathway, and *Smpd3*, which encodes nSMase2 in the ESCRT-independent pathway (Hessvik and Llorente 2018). Retinal lysates from dim-reared and 5-day photo-oxidative damaged retinas as well as lysates from GW4869 and DMSO-injected photo-oxidative damaged retinas were used. The expression of *Pdcd6ip* and *Smpd3* was significantly increased in 5-day photo-oxidative damaged retinas compared to dim-reared controls (Figure 3F). Conversely, *Pdcd6ip* and *Smpd3* were found to be significantly reduced in GW486-injected retinas compared to DMSO-injected controls (Figure 3G). Taken together these results show that GW4869 can be used both *in vitro* and *in vivo* as an effective inhibitor of exosome production. They further suggest that under stress conditions, exosomal communication may be necessary for photoreceptor cell survival.

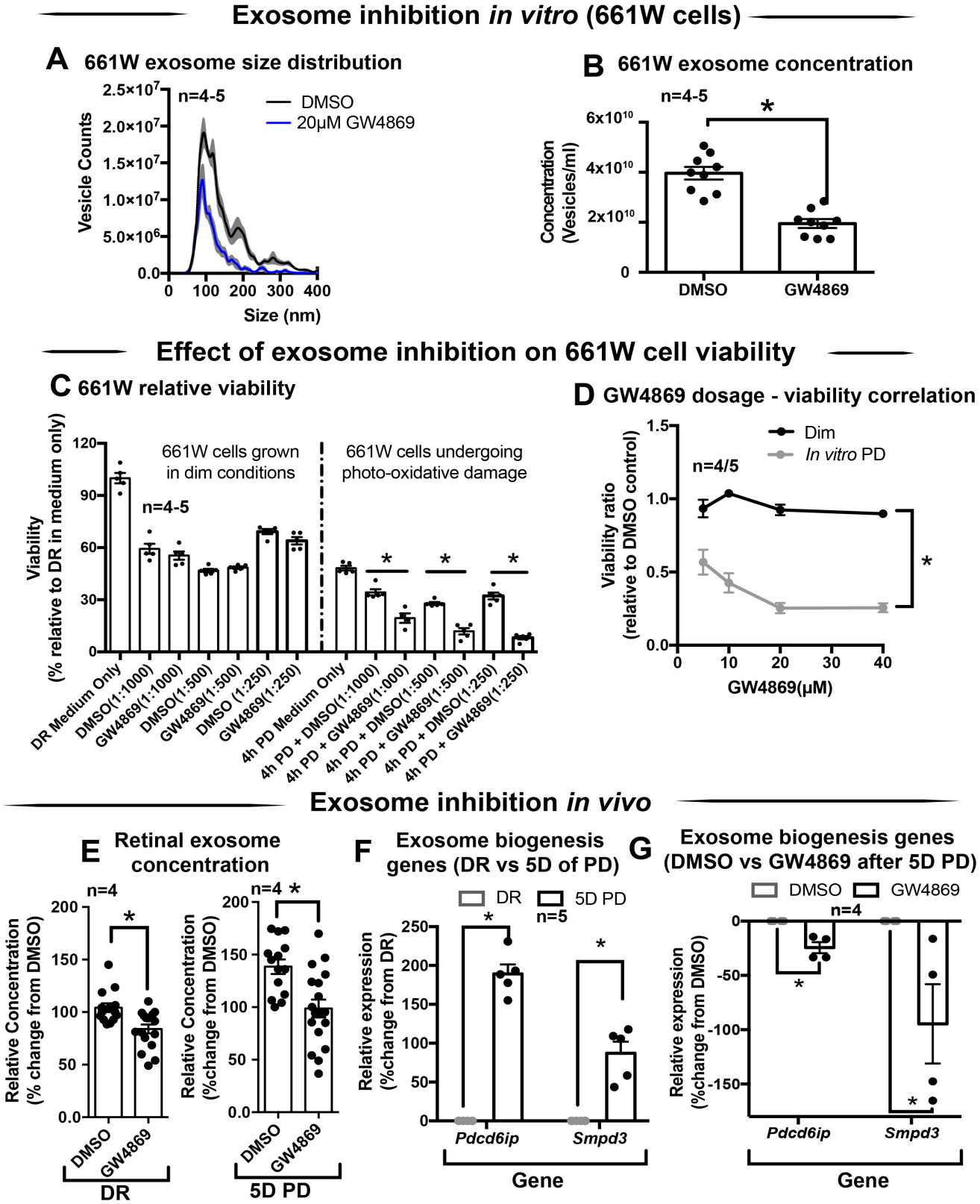

Figure 3: GW4869 inhibits biogenesis of retinal exosomes.

(A-B) Exosomes isolated from 661W photoreceptor-like cells in the presence of exosome inhibitor GW4869 (20μM) or DMSO control for 24 hours showed a significant reduction in

concentration, as measured by NanoSight NS300. ($P<0.05$, n=4-5). **(C)** MTT assay to determine viability of 661W cells treated with increasing concentrations of GW4869 or DMSO. Results demonstrated no dose response in viability levels for either treatment under dim conditions, however significant dose-dependent reduction in cell viability when treated with GW4869 under PD conditions ($P<0.05$). **(D)** The viability ratio ($viability_{GW4869}$ / $viability_{DMSO}$) of 661W cells treated with increasing concentrations of GW4869 in dim conditions or under 4 hours PD showed no change while in dim conditions, however is reduced between doses of 0-20µM GW4869 before reaching a plateau by 40µM while in PD conditions. **(E)** Nanotracking analysis (NanoSight NS300) quantification revealed a significant reduction in the concentration of exosomes isolated from both DR and 5D PD retinas following 5 daily intraperitoneal injections of GW4869 compared to respective DMSO controls ($P<0.05$, n=5). The expression of exosome biogenesis genes *Pdcd6ip* and *Smpd3* as measured by qRT-PCR was **(F)** significantly increased following 5D PD relative to DR controls ($P<0.05$, n=4) and **(G)** significantly reduced following daily injections of GW4869 while undergoing 5D PD, relative to DMSO injected controls ($P<0.05$, n=4).

3.4 Exosome inhibition reduces retinal function in dim-reared mice

The effect of GW4869-mediated exosome inhibition on retinal health was investigated in dim-reared mice. Retinal function was assessed using electroretinography (ERG). We show that GW4869-treated mice had reduced retinal function for both a-wave and b-wave measures (Figure 4A-B), compared to DMSO injected controls. To investigate this further, we measured photoreceptor cell death by counting $TUNEL^+$ cells in the outer nuclear layer (ONL). The inflammatory response was also measured by counting $IBA\text{-}1^+$ cells in the outer retina. No significant difference in either measure was observed between GW4869-injected and DMSO treated retinas (Figure 4C-E). Additionally, photoreceptor cell death was also assessed by measuring the ratio of ONL thickness to total retinal thickness from OCT images. No significant difference was detected between the two groups (Figure 4F-G). Overall, while GW4869 impaired retinal function in dim-reared mice, no difference was observed in histological measures between GW4869-injected mice and DMSO controls over the 5-day period investigated.

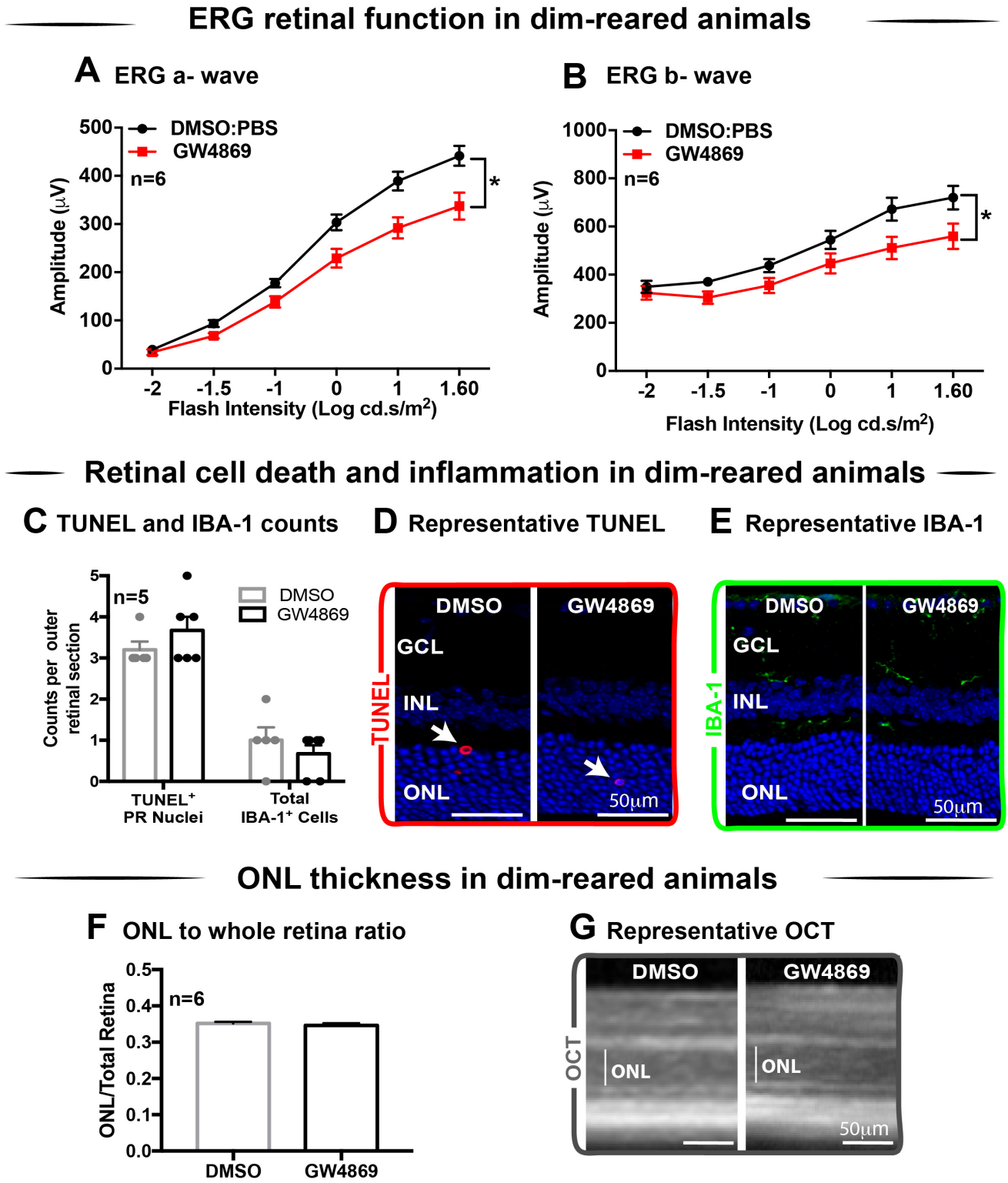

Figure 4: **Exosome inhibition via the use of GW4869 in dim-reared mice reduces retinal function**

Following 5 daily intraperitoneal injections of GW4869 (1.25mg/kg), retinal ERG function was significantly reduced for both **(A)** a-wave and **(B)** b-wave responses, compared to DMSO

controls in DR mice ($P<0.05$, n=6). **(C)** No significant changes were seen in either the number of TUNEL$^+$ cells in the outer nuclear layer, or in the number of IBA-1$^+$ cells in the outer retina following 5 daily intraperitoneal injections of GW4869 compared to DMSO controls ($P>0.05$, n=5). Representative confocal images show **(D)** TUNEL$^+$ cells (white arrows) and **(E)** IBA-1$^+$ cells in the outer retina in both GW4869 and DMSO injected DR mice. **(F)** There was no change in ONL thickness (represented as ratio to total retinal thickness), as measured by ocular coherence tomography (OCT) between GW4869 or DMSO injected DR mice ($P>0.05$, n=6). **(G)** Representative images of OCT scans show ONL thickness (white line) in GW4869 and DMSO injected DR mice. Scale bars = 50µM

3.5 Exosome inhibition reduces retinal function and increases cell death and immune cell recruitment in 5-day photo-oxidative damaged mice

Given the reduction in ERG responses in GW4869-treated dim-reared mice, the effect of exosome inhibition was further investigated in mice subjected to 5 days of photo-oxidative damage. GW4869-injected 5-day photo-oxidative damaged mice showed significantly reduced retinal function for both a-wave and b-wave measures (Figure 5A-B), compared to DMSO controls. Interestingly, and contrasting to GW4869-treated dim-reared mice, we observed significantly higher levels of photoreceptor cell death (TUNEL$^+$) and immune cell recruitment (IBA-1$^+$) in GW4869-injected 5-day photo-oxidative damaged mice compared to DMSO controls (Figure 5C). The increased number of IBA-1$^+$ cells in the outer retina included a higher ratio of amoeboid to ramified microglia and an increased presence of subretinal macrophages (Figure 5C). Further, there was a significant thinning of both the ONL and INL, indicating higher levels of cell death in GW4869-treated mice (Figure 5D). However, no difference in the thickness of the GCL was observed (Figure 5D). Increased levels of photoreceptor cell death in GW4869-injected photo-oxidative damage mice compared to DMSO controls was further demonstrated by a reduction of photoreceptor nuclei in the ONL (Figure 5E). Representative confocal images demonstrate an increase in photoreceptor cell death with significantly more TUNEL$^+$ cells and thinner ONL (Figure 5F), as well as increased IBA-1$^+$ cells (Figure 5G), in GW4869-treated mice compared to controls. Taken together these results show that exosome inhibition in retinas subjected to photo-oxidative damage causes reduced retinal function, concomitant with increased photoreceptor cell death and increased recruitment and activation of microglia/macrophages. This possibly indicates that reduced exosomal communication impairs regulation of the immune response in the retina.

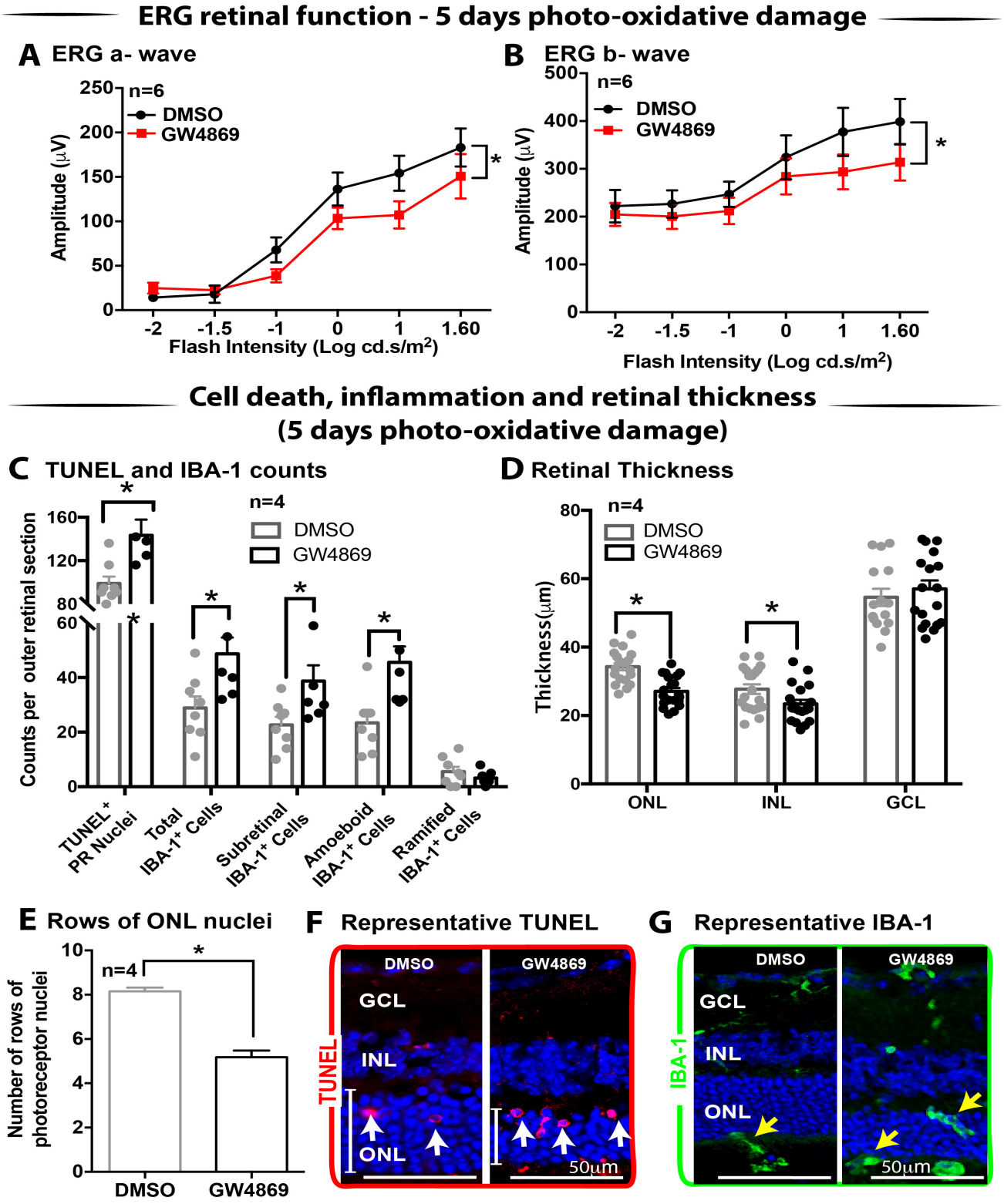

Figure 5: Exosome inhibition via the use of GW4869 in mice subjected to 5 days photo-oxidative damage reduces retinal function and increases cell death and immune cell recruitment.

Following 5 daily intraperitoneal injections of GW4869 (1.25mg/kg), retinal ERG function was significantly reduced for both **(A)** a-wave and **(B)** b-wave responses, compared to DMSO

controls in 5D PD mice (P<0.05, n=6). (**C**) There was a significant increase in the number of TUNEL$^+$ cells in the ONL, as well as a significant increase in the total number, number of subretinal, and number of amoeboid but not ramified IBA-1$^+$ cells in the outer retina in GW4869-injected mice compared to DMSO controls following 5D PD (P<0.05, n=4). **(D)** There was a significant reduction in the thickness of the ONL and INL of GW4869-injected 5D PD mice compared to DMSO controls (P<0.05, n=4), however, no change was observed in the thickness of the GCL between these groups (P>0.05, n=4). **(E)** The number of photoreceptor row nuclei in the ONL was also significantly reduced in GW4869-injected 5D PD mice compared to DMSO controls (P<0.05, n=4). Representative confocal images show **(F)** increased levels of TUNEL$^+$ cells (while arrow) and reduced ONL thickness (white line) as well as **(G)** increased number of IBA-1$^+$ cells in the outer retina, in GW4869-injected mice following 5 days of PD. Scale bars = 50µM.

3.6 Retinal exosomes of dim-reared and 5-day photo-oxidative damaged populations show no differential miRNA expression.

To obtain pure exosome-derived RNA, exosomes isolated from dim-reared and 5-day photo-oxidative damaged retinas were treated with RNaseA prior to RNA isolation to remove potential contaminating RNA species attached to the outside. Bioanalyzer electropherograms show that RNaseA treatment successfully removed contaminating RNA, whereas exosomal RNA was protected. Further, retinal exosomal RNA was enriched for RNA species between 10 to 40 nucleotides (Figure S2).

A two-dimensional principal component analysis (PCA) was carried out to identify global trends in the miRNA profile of both groups (Figure 6A). No clustering of the samples was observed, suggesting that the miRNA contents of retinal exosomes were not substantially altered following photo-oxidative damage. Hierarchical clustering analysis (HCA) further illustrated this point, with no significant clustering between dim-reared and 5-day photo-oxidative damage groups (Figure 6B). In line with the PCA and HCA, differential expression analysis revealed that only miR-1249-3p was differentially expressed (p-value = 0.046, fold change = -2.08) (Figure 6C). However, when adjusting for multiple comparisons (Benjamini-Hochberg), this miRNA did not pass the significance threshold (Table S1).

A total of 154 miRNAs were detected in retinal exosomes (Table S1) showing a similar mean count distributions in both groups (Figure 6D). The top 10 most highly expressed miRNAs were consistent in both dim-reared and 5-day photo-oxidative damaged retinal exosomes, and accounted for approximately 67% of the total (Figure 6E). MiR-124-3p was the

most abundant exoMiR representing 17.5% and 16.3% in dim-reared and 5-day photo-oxidative damaged retinal exosomes, respectively (Figure 6E). Four members of the let-7 family (let-7c-5p, let-7a-5p, let-7b-5p and let-7f-5p) as well as miR-183-5p, miR-125a-5p, miR-125b-5p, miR-706 and miR-204-5p comprised the rest of the top 10 most highly abundant exoMiR (Figure 6E).

Considering that exosomal miRNAs were not altered following 5 days of photo-oxidative damage and that the top 10 most abundant miRNAs accounted for 67% of the total exosomal miRNAome, we focused on these top 10 exoMiRs. A network analysis was performed to understand the interactions between the top 10 exoMiRs and the retinal transcriptome (Table S2). This revealed that eight miRNAs form a regulatory network containing 1326 targets (Figure 6F), of which, miR-124-3p, mir-706 and let-7b-5p, have 484, 267 and 376 predicted interactions with retinal transcripts, respectively (Table S3). These predicted targets were used for enrichment analyses against WikiPathways (mouse pathway annotation) and DisGeNET (database containing gene-disease associations) on the Enrichr platform. A total of 49 pathways were significantly over-represented in WikiPathways (Table S4). Notably, pathways pertaining to inflammatory processes including IL-1 to IL-6 signaling, Toll-like receptor signaling and chemokine signaling (Figure 6G) showed a significant enrichment. Pathways related to cell survival and motility were also significantly enriched (Figure 6H). DisGeNET database analysis revealed a significant association between exoMiR targets and 6 retinal diseases (Figure 6I, and Table S5), with the majority associated with an inflammatory and/or proliferative profile. In summary, exosomal miRNA cargo remains stable in the degenerating retina but the most abundant miRNA in exosomes are predicted to modulate inflammation, cell death responses and cellular motility pathways.

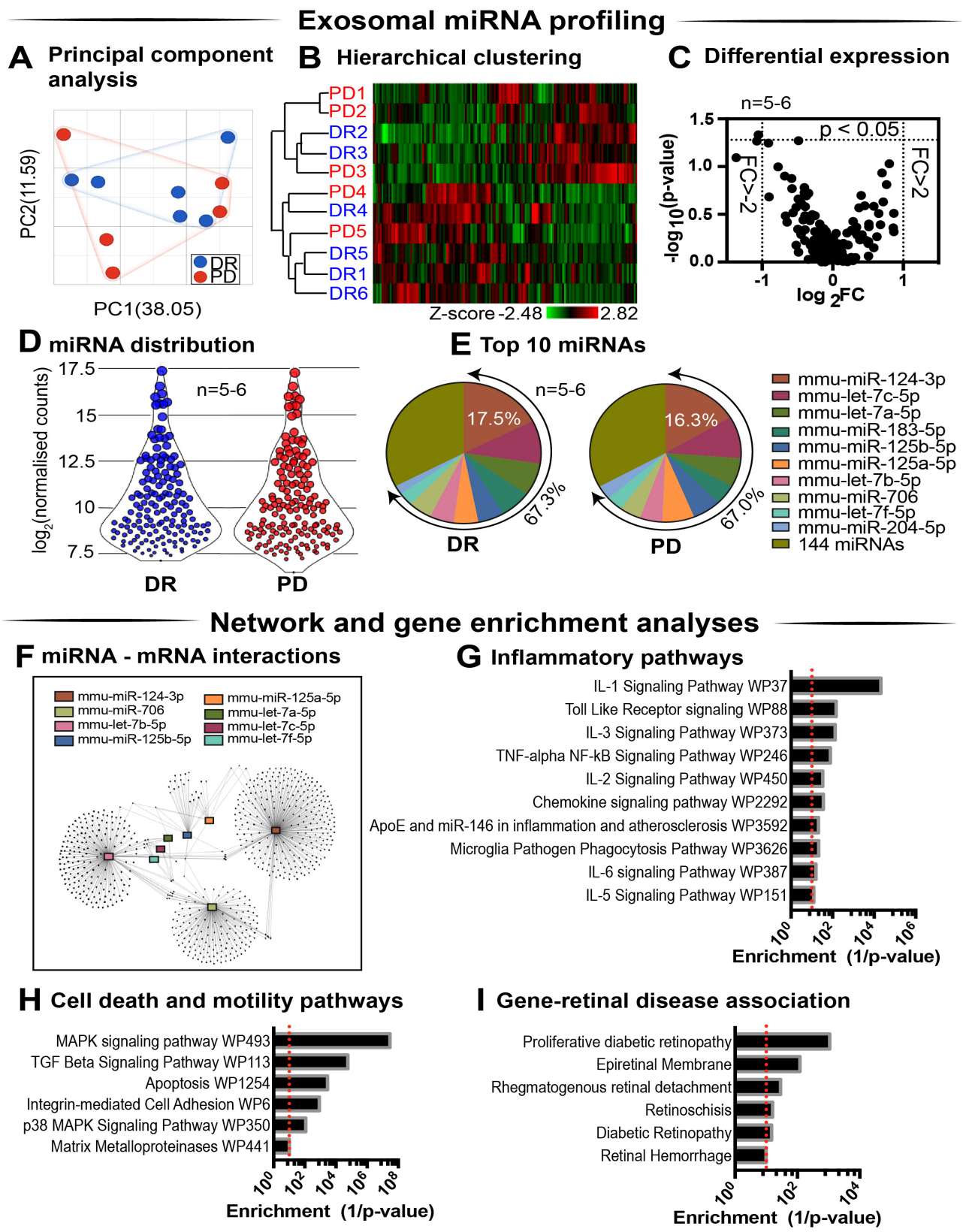

Figure 6. Exosomal miRNA profiling and enrichment analysis.
(A) Principal component analysis and **(B)** hierarchical clustering analysis showed no evident grouping of exoMiR in DR and 5D PD samples and identified no outliers. **(C)** Volcano plot

indicating that no differential analysis was observed in exosomes from DR and 5D PD retinas ($P>0.05$, n=5-6). **(D)** Violin plots showing the distribution of miRNA transcripts in exosomes from DR and 5D PD retinas (n=5-6). Each data point represents the $\log_2$ transformed average number of counts for each miRNA retained after removing miRNAs with low expression and the size of each point is proportional to the average expression value of each miRNA. Exosomes from both DR and 5 days PD retinas contain similar amounts of miRNA transcripts with low, medium and high expression. **(E)** The top 10 most abundant miRNA were conserved in retinal exosomes from DR and 5 days PD retinas and accounted for approximately 67% of the total counts. **(F)** miRNet network analysis using the top 10 most highly expressed exoMiRs showed that 8 out of the top 10 miRNAs form an interconnected network, with miR-124-3p, miR-706 and let-7b-5p having the largest number of predicted targets. Pathway analysis was performed using the predicted targets of the 8 miRNAs included in this network yielding significantly enriched pathways ($p<0.05$) pertaining to **(G)** inflammatory processes and oxidative stress as well as **(H)** cell survival and motility. **(I)** Enrichment analysis was also performed against DisGeNet (database containing gene-disease associations) revealing that a number of retinal diseases were significantly associated with the targets of exoMiRs ($P<0.05$).

3.7 Exosomes mediate the translocation of miR-124-3p from the outer to inner retina during photo-oxidative damage-induced retinal degeneration.

Following photo-oxidative damage, miRNA-124-3p translocates from the photoreceptor inner segments adjacent to the outer limiting membrane, to the inner nuclear layer (Chu-Tan, Rutar et al. 2018). We hypothesized that exosomes may mediate the transportation of miRNA, including miR-124-3p, through the retina during damage. To test this, *in situ* hybridization of miR-124-3p was performed on retinal cryosections from mice injected daily with GW4869 and subjected to 5 days of photo-oxidative damage. As previously reported (Chu-Tan, Rutar et al. 2018), miR-124-3p expression was significantly increased in the INL after 5 days photo-oxidative damage compared to dim-reared controls (Figure 7A-B). Interestingly, GW4869 treatment significantly reduced photo-oxidative damaged-induced miR-124-3p expression in the INL (Figure 7C-D). This indicates that the within-retinal movement of miR-124-3p in response to photo-oxidative damage is mediated by exosomes. Given the increased levels of cell death and inflammation in mice treated with GW4869, we speculate that exosomal shuttling of miRNA including miR-124-3p is required for normal retinal homeostasis and immune modulation.

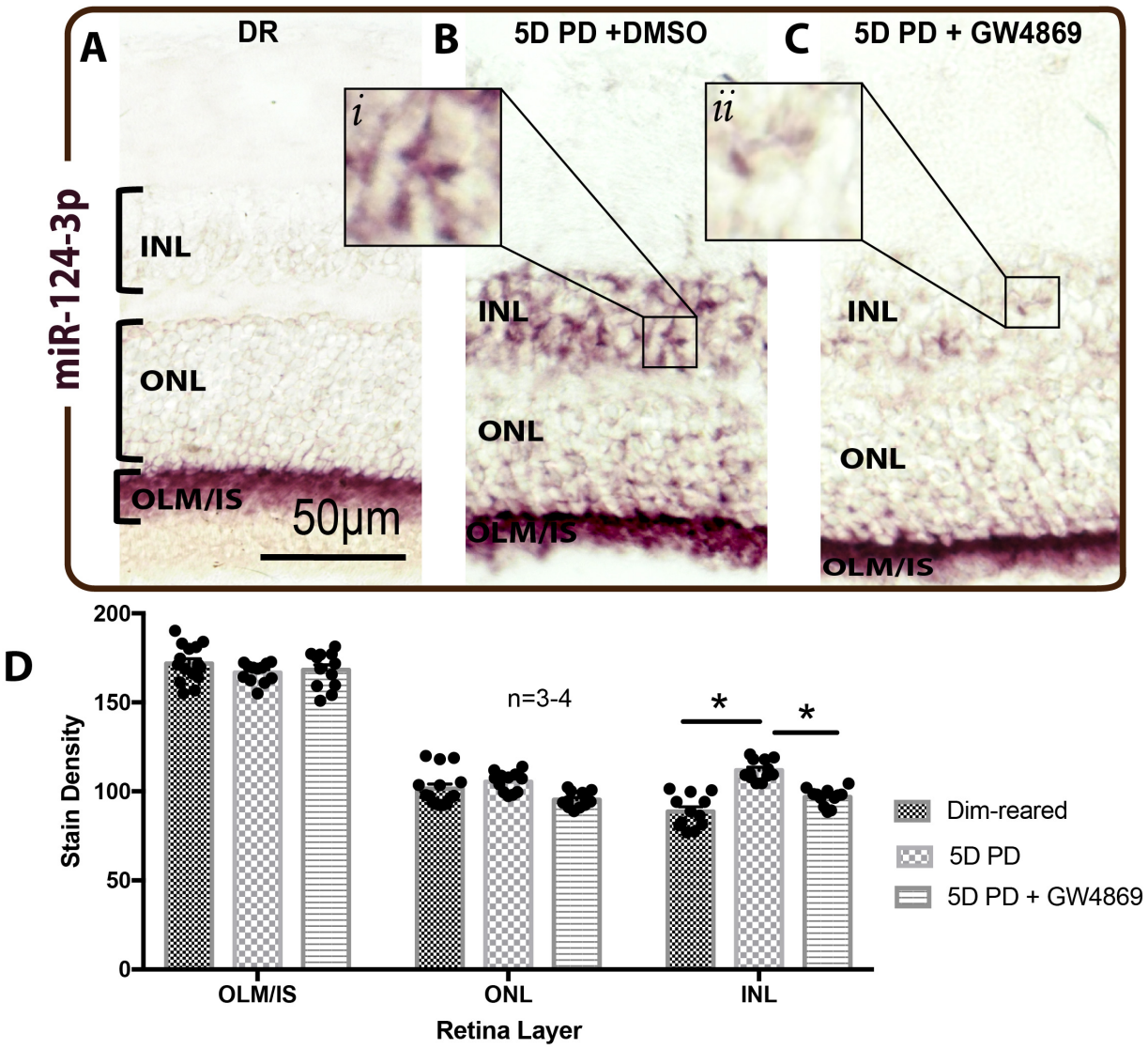

Figure 7: **Exosomes mediate the translocation of miR-124-3p from the outer to inner retina during photo-oxidative damage-induced retinal degeneration.**

(A) Using *in situ* hybridization, miR-124-3p expression in DR retinal cryosections was localized to the outer limiting membrane/photoreceptor inner segments (OLM, IS), however **(B)** following 5D PD, miR-124-3p was seen in the INL (inlet, i). **(C)** Following intraperitoneal administration of GW4869 exosome inhibitor, miR-124-3p expression is significantly reduced in the INL (inlet, ii). **(D)** Densitometry analysis of miR-124-3p in retinal layers. Scale bar = 50µM.

4 Discussion

This study describes for the first time, the isolation and characterization of mouse retinal exosomes and the important role they play in retinal health and degeneration. We demonstrate four key findings from this study: Firstly, we demonstrate that exosomes isolated from mouse retinas decrease in concentration progressively as a consequence of retinal degeneration. Secondly, we show that partial exosome depletion, via systemic administration of the exosome biogenesis inhibitor GW4869, resulted in reduced retinal function in the normal retina and further exacerbated functional losses in mice subjected to photo-oxidative damage. Notably, significant photoreceptor cell death and inflammation were observed in GW4869-injected mice undergoing photo-oxidative damage, which was mirrored *in vitro* by 661W photoreceptor-like cells displaying increased susceptibility to photo-oxidative damage following exosome inhibition. Thirdly, we used small RNA sequencing and bioinformatic analyses to report on the potential regulatory roles of exosomal miRNAs in retinal degeneration. Lastly, using the exosome-abundant miRNA miR-124-3p as a measure, we provide evidence that retinal exosomes are involved in the dynamic cell-to-cell transfer of miRNA in the degenerating retina. Taken together, we propose that retinal exosomes and their miRNA cargo play an essential role in maintaining retinal homeostasis through immune-modulation.

4.1 Photoreceptor cell death is associated with reduced exosome bioavailability

Previous studies have demonstrated that miRNA-laden exosomes are found in abundance in the CNS and are central to cell-to-cell communication (Fauré, Lachenal et al. 2006, Lachenal, Pernet-Gallay et al. 2011). Although it is unclear which retinal cell type(s) exosomes isolated in this work are secreted by, our evidence supports a photoreceptor-derived contribution. We demonstrate a progressive decrease in exosome numbers during photo-oxidative damage, which correlates with increasing levels of photoreceptor cell death as previously described in this model (Natoli, Jiao et al. 2016). Therefore, we attribute the decrease in isolated retinal exosomes to a loss of photoreceptors. In addition, the high abundance of photoreceptor prominent miRNAs miR-124-3p (Chu-Tan, Rutar et al. 2018) and miR-183-5p (Xiang, Chen et al. 2017) in isolated retinal exosomes, further attests to a potential photoreceptor origin, with miR-124-3p comprising 17.5% and 16.3% of the total ExoMiRnome in normal and damaged retinas, respectively.

Previous studies by Vidal-Gil et al. (2019) report that the exosome protein marker CD9 was localized to the photoreceptor inner segments and ONL, further supporting a photoreceptor-origin hypothesis. However, it should be noted that CD9 was also found in the INL, GCL and choroid. Using a genetic model (*rd10* mice) of retinitis pigmentosa, which results in progressive rod photoreceptor-specific cell death (Gargini, Terzibasi et al. 2007), Vidal-Gil et al. (2019) showed that EVs isolated from retinal explants contain rhodopsin protein. This exosomal rhodopsin expression increased following photoreceptor rescue. Therefore, the authors describe EV secretion as a function of photoreceptor cell death, with significantly lower levels of CD9 expressing vesicles isolated from *rd10* mouse retinas at postnatal day 18 (P18) compared to at P16 (Vidal-Gil, Sancho-Pelluz et al. 2019). Taken together these results demonstrate a clear relationship between retinal exosome secretion and photoreceptor cell survival, suggesting a significant exosome population may derive from photoreceptors in the retina.

Contrary to our findings, it is well established that a pro-oxidative stress or a proinflammatory environment often results in the increased release of exosomes (Lehmann, Paine et al. 2008, Essandoh, Yang et al. 2015, Benedikter, Weseler et al. 2018, Hessvik and Llorente 2018). We do observe increased expression of exosome biogenesis genes *Pdcd6ip* and *Smpd3* in retinal lysates following 5 days of photo-oxidative damage. We therefore suggest that all retinal cells including photoreceptors, as demonstrated by Vidal et al. (2019), may be potentially increasingly releasing exosomes as a consequence of the heightened presence of inflammatory and oxidative stress stimuli created in response to acute retinal degenerations. Further, we hypothesize that photoreceptors, as the most abundant retinal cell type, are the largest contributor to the pool of retinal exosomes and thus their loss leads to a net decrease in the total bioavailability of retinal exosomes. Independent isolation and quantification of exosomes from each major retinal cell type may shed some light in this regard and will be investigated in the future.

Alternatively, it is possible that in response to excessive light, increased numbers of retinal exosomes are mobilized as early responders to stress. However, even by 1 day of photo-oxidative damage, exosomes have already been depleted past a homeostatic level, ensuing an inflammatory response. Further, as we previously demonstrated the translocation of miR-124-3p to the INL within 24 hours of damage (Chu-Tan, Rutar et al. 2018), it seems likely that exosomal transport of this miRNA happened progressively before this time point as a rapid

response to stress. In fact, (Krol, Busskamp et al. 2010) demonstrated that photoreceptor-specific miRNAs such as miR-183/182/96 as well as miR-204 and miR-211 are modulated in response to light exposure as short as 3 hours. We also identified mir-183/182/96, miR-204 and miR-211 in retinal exosomes however, while Krol and colleagues do not propose a mechanism responsible for the miRNA turnover observed in their work, our work presented here suggests that exosomes may be involved. Quantifying exosome secretion during early stress responses is required to determine if exosome depletion is a cause or consequence of retinal degeneration, and represents an important piece of the therapeutic puzzle.

4.2 Retinal exosomes as mediators of immuno-modulation.

Regardless of origin, to date the role that exosomes play in retinal health and disease is still largely unclear. Results from this work strongly support a mechanism by which retinal exosomes mediate homeostasis and immuno-modulation, with the inhibition of exosomes using GW4869 both *in vitro*, and *in vivo*, resulting in increased cell death, as well as recruitment and activation of microglia/macrophages. Importantly these observations were only evident under stress conditions, with both control 661W cells and dim-reared retinas displaying no major signs of cell death or inflammation following exosome-inhibition in the absence of photo-oxidative damage. We suggest that unlike in the degenerating retina, that exosome inhibition had no major effects on cell health. This is likely to be a consequence of the experimental paradigm used in this study and the short period of inhibition, or alternatively could indicate that under stress exosomal communication is necessary for cell survival.

We hypothesize that as a consequence of longer-term exosome inhibition, inadequate translocation of exoMiR cargo would likely result in the dysregulation of immune pathways. In this present study, we demonstrate that in mice treated with GW4869, miR-124-3p, the most highly expressed miRNA in isolated retinal exosomes, was prevented from translocating from photoreceptors to the inner retina. We have previously reported that miR-124-3p translocation was required for the suppression of C-C Motif Chemokine Ligand 2 (Ccl2), acting as an anti-inflammatory regulator to prevent the recruitment of both resident and peripheral microglia/macrophages to the site of damage (Chu-Tan, Rutar et al. 2018). We propose therefore that insufficient gene regulation from miR-124-3p due to exosome reduction is one

factor contributing to the increased presence of immune cells and inflammation as a consequence of retinal degenerations.

To further support the hypothesis that retinal exosomes mediate homeostasis and immune responses, network and pathway analysis of retinal exoMiRs revealed that the top 10 miRNA were associated with the regulation of inflammatory and cell survival pathways. For example, our network analysis indicates that the top 10 miRNA are controlling genes associated with Interleukin and chemokine signaling, with both of these biological pathways involved in a plethora of retinal degenerative diseases (Rutar, Natoli et al. 2015, Wooff, Man et al. 2019). Moreover, MAPK signaling and TGF-β have also been shown to play pivotal roles in the development of retinal degenerations (Kyosseva 2016, Wang, Li et al. 2018), with both pathways showing a strong association with the targetome of the top 10 most highly expressed exoMiRs. As the top 10 miRNAs in both dim-reared and photo-oxidative damage retinal exosomes make up approximately 70% of the total exoMiRnome, it is not surprising that a reduction in exosome numbers during degeneration could lead to immune dysfunction due to inadequate gene regulation. In fact, enrichment analysis of retinal exoMiR revealed significant associations with retinal degenerative diseases such diabetic retinopathy, retinal detachment and retinal hemorrhage further highlighting their potential involvement in modulating retinal inflammatory diseases.

From these collective findings, we propose that in normal retinal health, exosomes are secreted from photoreceptor cells, and are released to the surrounding retina to maintain a homeostatic environment. However, following photoreceptor cell death, we hypothesize that immune responses are no longer able to be regulated due to reduced exosome numbers and the bioavailability of miRNA cargo; leading to the upregulation of inflammatory pathways, infiltration and activation of microglia/macrophages and progressive retinal cell death (Figure 8); characteristic features of retinal degenerative diseases (Kauppinen, Paterno et al. 2016, Rivera, Holm et al. 2017, Rübsam, Parikh et al. 2018, Wooff, Man et al. 2019).

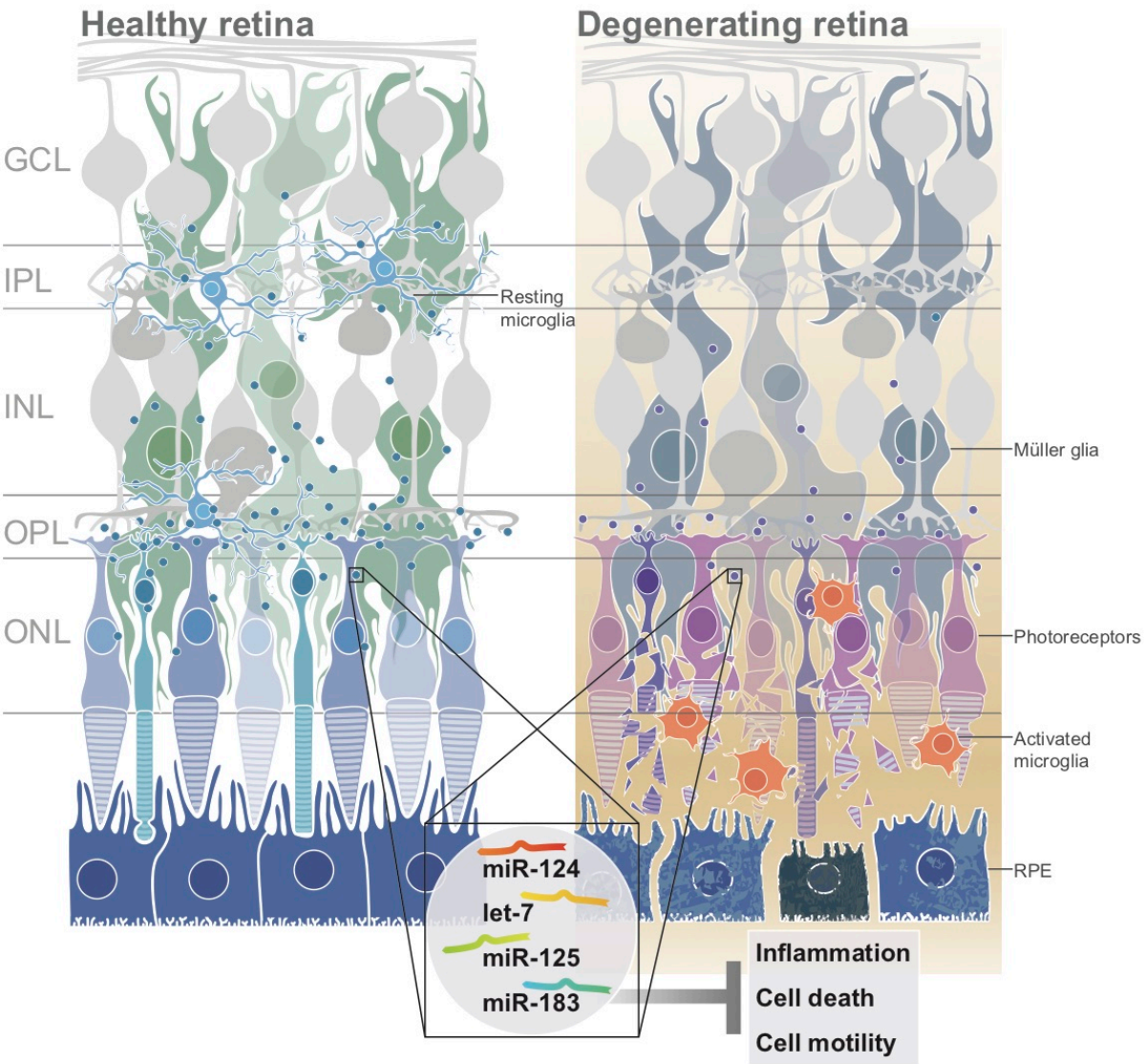

Figure 8: Proposed functional role of exosomes.

Under normal homeostatic conditions, exosomes laden with miRNA, including miR-124, let-7, miR-125 and miR-183, potentially originating from photoreceptors, are continuously trafficked between retinal neurons and glial cells. However, in retinal degenerations, a loss of photoreceptors leads to a decrease in exosome bioavailability, and consequently an insufficient transfer of exosomal miRNA cargo to their cell targets. As the retinal targetome of exoMiRs is associated with inflammation, survival and cell motility pathways, inadequate pathway regulation following exosomal depletion leads to exacerbated retinal damage.

4.3 Exosomes as mediators of phototransduction

In addition to a potential role as regulators of retinal homeostasis through immune modulation, we highlight a possible involvement of retinal exosomes in phototransduction. In both dim-reared and photo-oxidative damaged mice, exosome inhibition resulted in reduced

retinal function as measured by ERG. While we could attribute the loss of retinal function in photo-oxidative damage mice to increased levels of photoreceptor cell death and immune cell recruitment, dim-reared mice showed no detectable signs of either cell death or inflammation yet still demonstrated significantly lower functional responses.

While the role of exosomes in phototransduction in the retina is currently unknown, in the CNS the communication of exosomal cargo from oligodendrocytes and astrocytes has been reported to affect neurotransmission pathways (Antonucci, Turola et al. 2012, Fröhlich, Kuo et al. 2014, Pascua-Maestro, González et al. 2018). In particular, Fruhbeis et. al (2013) suggested that the exosome communication between oligodendrocytes and neuronal axons is triggered by glutamate release (Frühbeis, Fröhlich et al. 2013). While oligodendrocytes are not present in the retina, Müller glia perform a similar role, responsible for the reuptake of glutamate released from photoreceptors terminals and the synaptic clefts of second order neurons as part of normal phototransduction (Bringmann, Grosche et al. 2013). We speculate that, perturbations of exosomal communication systems could lead to aberrant glutamate reuptake by Muller cells and impaired signal transduction, explaining the observed reduction in retinal function of exosome-inhibited mice. However, this area requires further in-depth exploration.

4.4 The role of exosomes in retinal degenerative diseases and their potential as therapeutic gene therapy vehicles.

To date, little progress has been made in uncovering the role that exosomes may play in the progression of retinal degenerations, and further how we can utilize exosomes, their cargo, and/or biological targets in diagnostic panels and in therapeutic development. It has been recently shown in cell culture models (Kang, Bang et al. 2014, Atienzar-Aroca, Flores-Bellver et al. 2016, Zhang, Ma et al. 2019), that following high levels of oxidative stress (pathologically relevant to the onset of many retinal degenerative diseases), increased exosome numbers containing high expression of vascular endothelial growth factor receptor (VEGFR,) are secreted from a retinal pigmented epithelium (RPE) cell culture line (aRPE19) to promote neovascularization, a hallmark feature of several retinal pathologies (Atienzar-Aroca, Flores-Bellver et al. 2016). It has also been reported that exosomes containing retinal proteins were found in abundance in the vitreous humor of the mouse and human, demonstrating a level of communication that exists between these ocular tissues (Zhao, Weber et al. 2018). While it has yet to be discovered if there is any differential change in exosome composition or concentration

in the vitreous during retinal degenerative diseases, exosomes identified in the aqueous humor of AMD patients were found to contain a cross-over set of proteins also found in the culture medium of aRPE19 cells (Kang, Bang et al. 2014). This finding, while largely correlative, suggests that exosomes derived from the RPE may play a role in disease pathogenesis. Furthermore, these results demonstrate the possibility that access to exosome populations in biological fluids of the eye could provide a representation of what may be occurring in the retina and therefore serves a diagnostic potential.

Exosome based gene therapies are at the forefront of therapeutic development, with multiple clinical trials underway (Lener, Gimona et al. 2015, Sarko and McKinney 2017), including for the treatment of neurodegenerative diseases (Sarko and McKinney 2017, Mead and Tomarev 2020). However, their use for the treatment of retinal degenerations is largely in its infancy (reviewed in (Mead and Tomarev 2020). Hajrasouliha et. al (2013) provides evidence for the immunomodulatory properties of exosomes derived from cultured retinal astrocytes (Hajrasouliha, Jiang et al. 2013). Using a laser induced model of choroidal neovascularization Hajrasouliha et. al (2013), demonstrated that the periocular injection of astrocytic exosomes reduced the CCL2-dependent migration of macrophages to the lesion site and attenuated angiogenesis (Hajrasouliha, Jiang et al. 2013). As CCL2 has been implicated as a key chemokine in the pathogenesis of multiple retinal degenerative diseases (Newman, Gallo et al. 2012, Rutar, Natoli et al. 2012, Zuzic, Rojo Arias et al. 2019), and is a known target of miR-124-3p (Zuzic, Rojo Arias et al. 2019); exosome-based therapies that replenish retinal levels of this miRNA may prove efficacious as a possible therapeutic, as evidenced in other works (Chu-Tan, Rutar et al. 2018). In addition, exosomes derived from microglial cells and injected into the vitreous of mice subjected to oxygen-induced retinopathy showed protective effects, reducing avascular regions in the retina, VEGF expression, and photoreceptor apoptosis, compared to controls (Xu, Wu et al. 2019). It was hypothesized by these authors that exosomal-miR-24-3p mediated this protection against hypoxia-induced cell death (Xu, Wu et al. 2019).

The combined findings of our work uncover a novel role for retinal exosomes in both health and degeneration, unveiling a panel of exoMiR required for retinal homeostasis, and target networks of these gene regulators comprising inflammatory, oxidative stress and cell survival pathways. As we elude to retinal health requiring optimal levels of exosomes, and their cargo; replenishing exosome loads in the retina, itself may prove as efficacious therapy,

and will be the focus of future works. Further, both the unique exoMiR signature and downstream target pathways open additional avenues for therapeutic development.

5 Conclusion

Results from this work suggest that exosomes are released from photoreceptor cells to maintain retinal homeostasis. However, as a consequence of photoreceptor cell death, exosome secretion and/or bioavailability becomes reduced. Consequently, retinal exosomal cargo, which contains regulatory miRNA and other molecules, are unable to regulate immune responses, subsequently contributing to progressive retinal cell death. We hypothesis that this mechanism is likely to be involved in many retinal degenerative and inflammatory diseases.

Acknowledgements

This work would not have been possible without the support of the National Health and Medical Research Council of Australia (NHMRC: 1127705), Retina Australia, The Gordon and Gretel Bootes Foundation and The ANU Translational Fellowship.

These authors would also like to acknowledge the facilities and the scientific and technical assistance of Microscopy Australia at the Advanced Imaging Precinct, Australian National University. A facility that is funded by the University and State and Federal governments. In addition, the facilities and staff of the John Curtin School of Medical Research Biomolecular Research Facility (JCSMR, BRF, ACT, AUS).

Author Contributions

Conceptualization. YW, AC, RN; Methodology YW, AC, JCT, RN; Data analysis YW, AC, JCT, RN; Investigation YW, AC, RN; Writing – Original Draft YW, AC, RN; Writing – Review and Editing YW, AC, JCT, RAB, US, RN; Supervision RN, Funding Acquisition, RN

Declarations of Interest

The authors declare no competing interests.

6 Supplementary Figures

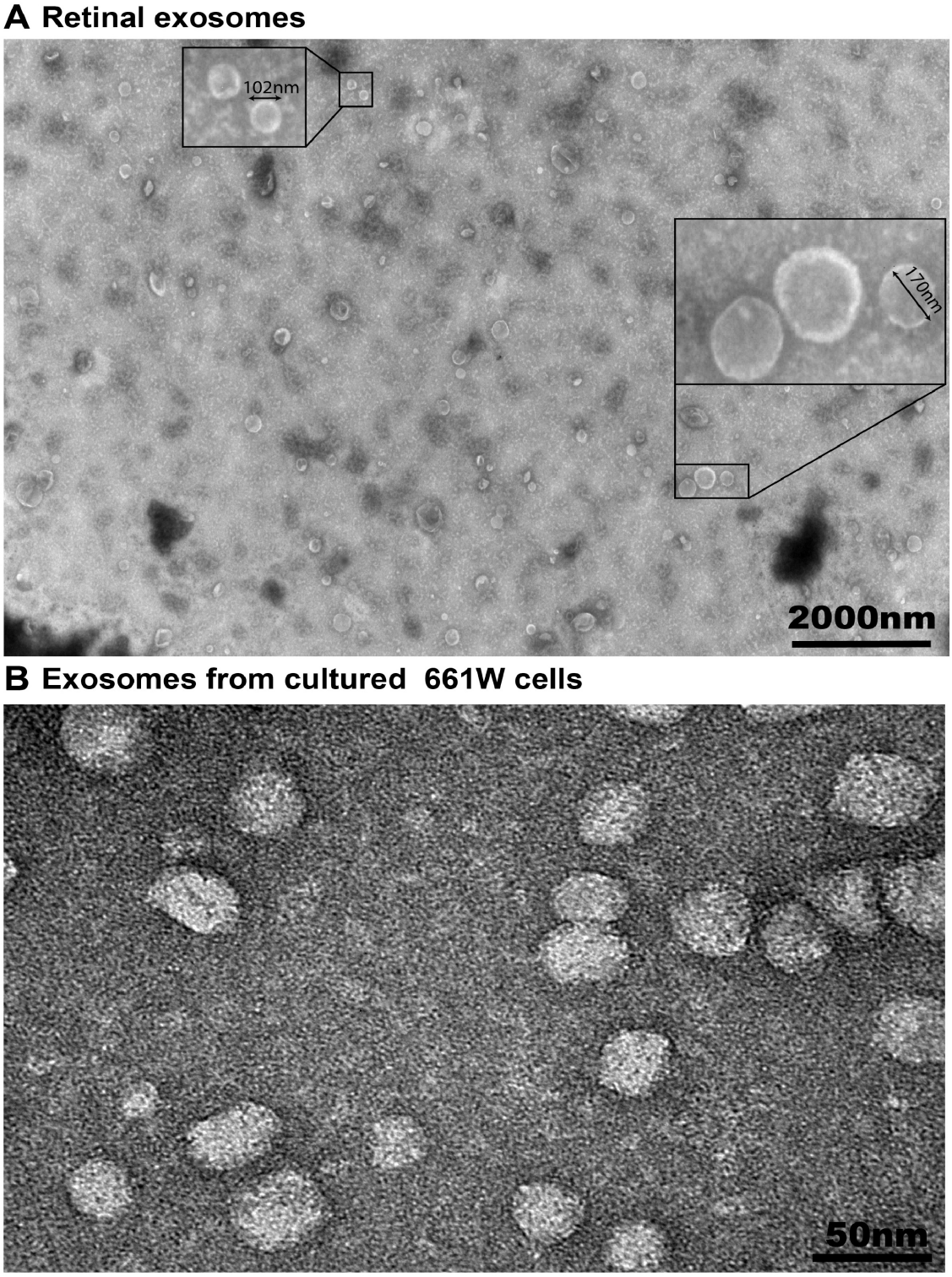

Figure S1. Representative TEM image showing isolated extracellular vesicles from **(A)** retinas and **(B)** 661W cells. Enlarged fields highlight the circular, cup-shape morphology and size of exosomes. Scale bar = 2000nm and 50nm.

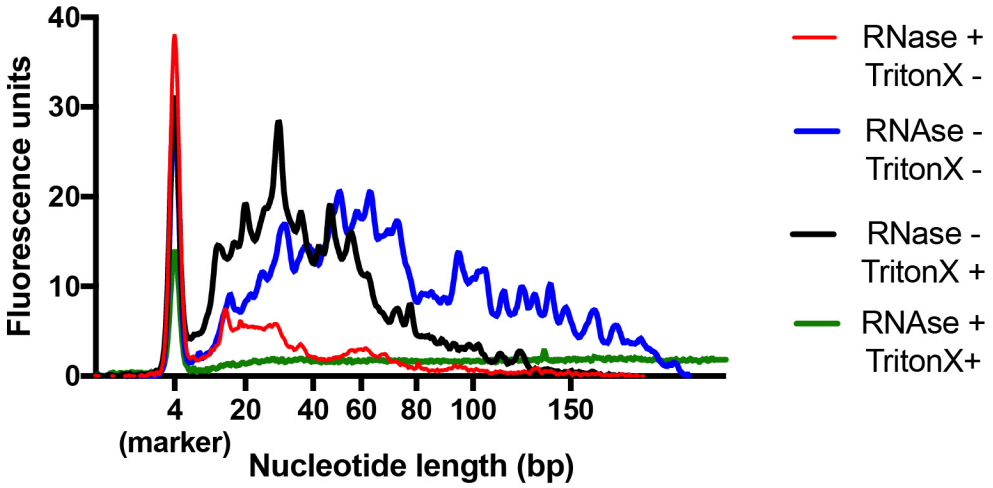

Figure S2. RNaseA treatment.

Exosomes were treated with RNaseA with or without Triton-X 100 for 30 mins then processed immediately for RNA extraction. Exosomes treated with RNAaseA without Triton-X 100 (red line) showed a decrease in the total amount of RNA compared with untreated exosomes (blue line), and total RNA (black line), indicating the presence of contaminating RNA. The RNA protected from RNaseA degradation (red line) was enriched for RNA species of 10 to 40 nucleotides (bp) in length. The simultaneous treatment with RNasA and Triton-X 100 (green line) completely ablated the signal, further demonstrating that exosomal RNA is protected from RNAseA degradation.

Read trimming, alignment and normalization

A Sequencing reads summary

Sample name	Total reads	Read length	Avg. read quality	% N	% GC
DR1	14,577,486	51.00	33.13	0%	43.77%
DR2	13,972,828	51.00	33.19	0%	44.37%
DR3	15,003,428	51.00	33.19	0%	44.72%
DR4	8,960,555	51.00	32.43	0%	41.65%
DR5	10,009,182	51.00	32.64	0%	42.05%
DR6	9,918,357	51.00	32.37	0%	42.67%
PD1	15,073,063	51.00	33.24	0%	45.01%
PD2	15,641,433	51.00	33.20	0%	45.43%
PD3	11,058,946	51.00	33.13	0%	44.18%
PD4	11,413,904	51.00	32.55	0%	41.06%
PD5	8,104,058	51.00	32.20	0%	42.43%

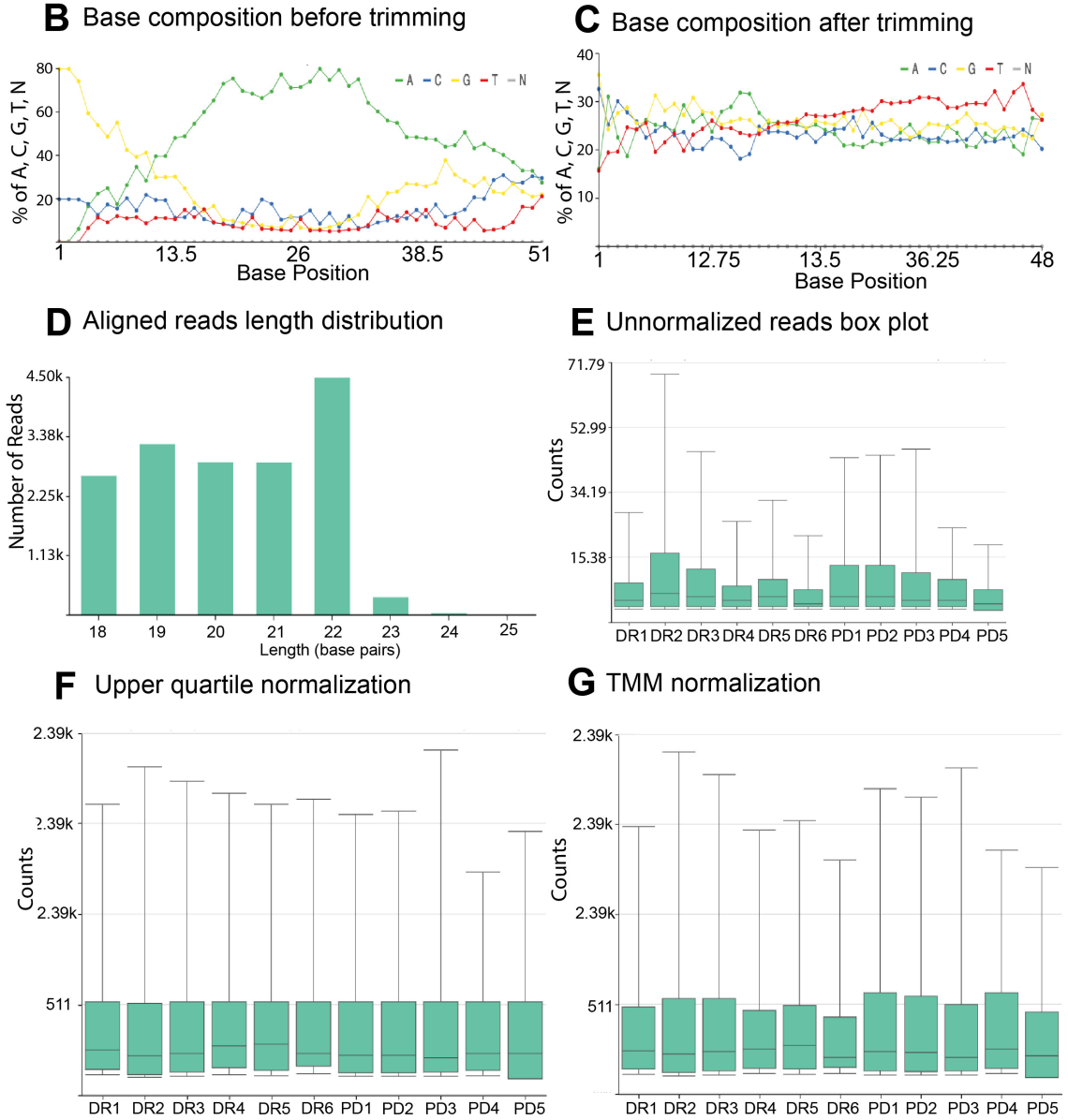

Figure S3. Sequenced reads processing, alignment and normalization. (A) Summary of the sequencing depth, read quality and GC content**. (B)** Representative raw read base composition shows the presence of an enriched poly-A tail (green line) and template switching nucleotide (first 3 base pairs). These features are incorporated during the CATS library preparation and thus their enrichment in the sequenced reads indicates the successful construction of the library.

(C) After trimming, every nucleotide was equally represented along the sequenced reads indicating the successful removal of library contaminants. **(D)** Reads aligning to miRbase v.22 (mature miRNA) had length distribution ranging from 18 to 24 nucleotides consistent with the length of annotated miRNAs. **(E)** After annotation, unnormalized counts were normalized using the **(F)** upper quartile (UQ) normalization or **(G)** Trimmed Means of M, with the former producing more similar means and distributions (each box-and whisker plot corresponds to a sample).

7 References:

Abels, E. R. and X. O. Breakefield (2016). Introduction to extracellular vesicles: biogenesis, RNA cargo selection, content, release, and uptake, Springer.

Abusamra, A. J., Z. Zhong, X. Zheng, M. Li, T. E. Ichim, J. L. Chin and W.-P. Min (2005). "Tumor exosomes expressing Fas ligand mediate CD8+ T-cell apoptosis." Blood Cells, Molecules, and Diseases **35**(2): 169-173.

Al-Ubaidi, M. R., J. G. Hollyfield, P. A. Overbeek and W. Baehr (1992). "Photoreceptor degeneration induced by the expression of simian virus 40 large tumor antigen in the retina of transgenic mice." Proceedings of the National Academy of Sciences **89**(4): 1194-1198.

Alexander, M., R. Hu, M. C. Runtsch, D. A. Kagele, T. L. Mosbruger, T. Tolmachova, M. C. Seabra, J. L. Round, D. M. Ward and R. M. O'Connell (2015). "Exosome-delivered microRNAs modulate the inflammatory response to endotoxin." Nature communications **6**: 7321-7321.

Anel, A., A. Gallego-Lleyda, D. de Miguel, J. Naval and L. Martínez-Lostao (2019). "Role of exosomes in the regulation of T-cell mediated immune responses and in autoimmune disease." Cells **8**(2): 154.

Antonucci, F., E. Turola, L. Riganti, M. Caleo, M. Gabrielli, C. Perrotta, L. Novellino, E. Clementi, P. Giussani, P. Viani, M. Matteoli and C. Verderio (2012). "Microvesicles released from microglia stimulate synaptic activity via enhanced sphingolipid metabolism." The EMBO journal **31**(5): 1231-1240.

Atienzar-Aroca, S., M. Flores-Bellver, G. Serrano-Heras, N. Martinez-Gil, J. M. Barcia, S. Aparicio, D. Perez-Cremades, J. M. Garcia-Verdugo, M. Diaz-Llopis and F. J. Romero (2016). "Oxidative stress in retinal pigment epithelium cells increases exosome secretion and promotes angiogenesis in endothelial cells." Journal of cellular and molecular medicine **20**(8): 1457-1466.

Bartel, D. P. (2009). "MicroRNAs: target recognition and regulatory functions." Cell **136**(2): 215-233.

Benedikter, B. J., A. R. Weseler, E. F. M. Wouters, P. H. M. Savelkoul, G. G. U. Rohde and F. R. M. Stassen (2018). "Redox-dependent thiol modifications: implications for the release of extracellular vesicles." Cellular and Molecular Life Sciences **75**(13): 2321-2337.

Bhome, R., F. Del Vecchio, G.-H. Lee, M. D. Bullock, J. N. Primrose, A. E. Sayan and A. H. Mirnezami (2018). "Exosomal microRNAs (exomiRs): Small molecules with a big role in cancer." Cancer letters **420**: 228-235.

Bringmann, A., A. Grosche, T. Pannicke and A. Reichenbach (2013). "GABA and Glutamate Uptake and Metabolism in Retinal Glial (Müller) Cells." Frontiers in endocrinology **4**: 48-48.

Chan, B. D., W.-Y. Wong, M. M.-L. Lee, W. C.-S. Cho, B. K. Yee, Y. W. Kwan and W. C.-S. Tai (2019). "Exosomes in Inflammation and Inflammatory Disease." PROTEOMICS **19**(8): 1800149.

Charlotte, L., M. V. Jose, M. Y. Derek and M. D. Sean (2016). "Microvesicles and exosomes: new players in metabolic and cardiovascular disease." Journal of Endocrinology **228**(2): R57-R71.

Chen, E. Y., C. M. Tan, Y. Kou, Q. Duan, Z. Wang, G. V. Meirelles, N. R. Clark and A. Ma'ayan (2013). "Enrichr: interactive and collaborative HTML5 gene list enrichment analysis tool." BMC bioinformatics **14**: 128-128.

Christopher, A. F., R. P. Kaur, G. Kaur, A. Kaur, V. Gupta and P. Bansal (2016). "MicroRNA therapeutics: Discovering novel targets and developing specific therapy." Perspectives in clinical research **7**(2): 68-74.

Chu-Tan, J. A., M. Rutar, K. Saxena, R. Aggio-Bruce, R. W. Essex, K. Valter, H. Jiao, N. Fernando, Y. Wooff, M. C. Madigan, J. Provis and R. Natoli (2018). "MicroRNA-124 Dysregulation is Associated With Retinal Inflammation and Photoreceptor Death in the Degenerating RetinaMicroRNA-124 Dysregulation in the Degenerating Retina." Investigative Ophthalmology & Visual Science **59**(10): 4094-4105.

Cypryk, W., T. A. Nyman and S. Matikainen (2018). "From Inflammasome to Exosome—Does Extracellular Vesicle Secretion Constitute an Inflammasome-Dependent Immune Response?" Frontiers in Immunology **9**: 2188.

Desdín-Micó, G. and M. Mittelbrunn (2017). "Role of exosomes in the protection of cellular homeostasis." Cell adhesion & migration **11**(2): 127-134.

Donoso, L. A., D. Kim, A. Frost, A. Callahan and G. Hageman (2006). "The role of inflammation in the pathogenesis of age-related macular degeneration." Survey of ophthalmology **51**(2): 137-152.

Erik Clarke, S. S.-M. (2017). "ggbeeswarm: Categorical Scatter (Violin Point) Plots."

Essandoh, K., L. Yang, X. Wang, W. Huang, D. Qin, J. Hao, Y. Wang, B. Zingarelli, T. Peng and G. C. Fan (2015). "Blockade of exosome generation with GW4869 dampens the sepsis-induced inflammation and cardiac dysfunction." Biochim Biophys Acta **1852**(11): 2362-2371.

Fan, Y., K. Siklenka, S. K. Arora, P. Ribeiro, S. Kimmins and J. Xia (2016). "miRNet - dissecting miRNA-target interactions and functional associations through network-based visual analysis." Nucleic acids research **44**(W1): W135-W141.

Fauré, J., G. Lachenal, M. Court, J. Hirrlinger, C. Chatellard-Causse, B. Blot, J. Grange, G. Schoehn, Y. Goldberg, V. Boyer, F. Kirchhoff, G. Raposo, J. Garin and R. Sadoul (2006). "Exosomes are released by cultured cortical neurones." Molecular and Cellular Neuroscience **31**(4): 642-648.

Fleshner, M. and C. R. Crane (2017). "Exosomes, DAMPs and miRNA: features of stress physiology and immune homeostasis." Trends in immunology **38**(10): 768-776.

Fröhlich, D., W. P. Kuo, C. Frühbeis, J.-J. Sun, C. M. Zehendner, H. J. Luhmann, S. Pinto, J. Toedling, J. Trotter and E.-M. Krämer-Albers (2014). "Multifaceted effects of oligodendroglial exosomes on neurons: impact on neuronal firing rate, signal transduction and gene regulation." Philosophical transactions of the Royal Society of London. Series B, Biological sciences **369**(1652): 20130510.

Frühbeis, C., D. Fröhlich, W. P. Kuo, J. Amphornrat, S. Thilemann, A. S. Saab, F. Kirchhoff, W. Möbius, S. Goebbels, K.-A. Nave, A. Schneider, M. Simons, M. Klugmann, J. Trotter and E.-M. Krämer-Albers (2013). "Neurotransmitter-Triggered Transfer of Exosomes Mediates Oligodendrocyte–Neuron Communication." PLOS Biology **11**(7): e1001604.

Gargini, C., E. Terzibasi, F. Mazzoni and E. Strettoi (2007). "Retinal organization in the retinal degeneration 10 (rd10) mutant mouse: a morphological and ERG study." The Journal of comparative neurology **500**(2): 222-238.

Gerritzen, M. J. H., D. E. Martens, R. H. Wijffels and M. Stork (2017). "High throughput nanoparticle tracking analysis for monitoring outer membrane vesicle production." Journal of extracellular vesicles **6**(1): 1333883-1333883.

Gupta, A. and L. Pulliam (2014). "Exosomes as mediators of neuroinflammation." Journal of neuroinflammation **11**: 68-68.

Hajrasouliha, A. R., G. Jiang, Q. Lu, H. Lu, H. J. Kaplan, H.-G. Zhang and H. Shao (2013). "Exosomes from retinal astrocytes contain antiangiogenic components that inhibit laser-

induced choroidal neovascularization." The Journal of biological chemistry **288**(39): 28058-28067.

Hessvik, N. P. and A. Llorente (2018). "Current knowledge on exosome biogenesis and release." Cellular and Molecular Life Sciences **75**(2): 193-208.

Hsu, M.-Y., C.-C. Chiu, J.-Y. Wang, C.-T. Huang, Y.-F. Huang, J.-C. Liou, C. Chen, H.-C. Chen and C.-M. Cheng (2018) "Paper-Based Microfluidic Platforms for Understanding the Role of Exosomes in the Pathogenesis of Major Blindness-Threatening Diseases." Nanomaterials (Basel, Switzerland) **8** DOI: 10.3390/nano8050310.

Huang, C., K. P. Fisher, S. S. Hammer, S. Navitskaya, G. J. Blanchard and J. V. Busik (2018). "Plasma exosomes contribute to microvascular damage in diabetic retinopathy by activating the classical complement pathway." Diabetes **67**(8): 1639-1649.

Jain, G., A. Stuendl, P. Rao, T. Berulava, T. Pena Centeno, L. Kaurani, S. Burkhardt, I. Delalle, J. Kornhuber, M. Hüll, W. Maier, O. Peters, H. Esselmann, C. Schulte, C. Deuschle, M. Synofzik, J. Wiltfang, B. Mollenhauer, W. Maetzler, A. Schneider and A. Fischer (2019). "A combined miRNA–piRNA signature to detect Alzheimer's disease." Translational Psychiatry **9**(1): 250.

Jan, A. T., M. A. Malik, S. Rahman, H. R. Yeo, E. J. Lee, T. S. Abdullah and I. Choi (2017). "Perspective Insights of Exosomes in Neurodegenerative Diseases: A Critical Appraisal." Frontiers in aging neuroscience **9**: 317-317.

Janik-Papis, K., M. Ulińska, A. Krzyzanowska, E. Stoczyńska, A. Borucka, K. Woźniak, Z. Małgorzata, J. Szaflik and J. Blasiak (2009). "Role of oxidative mechanisms in the pathogenesis of age-related macular degeneration." Klinika oczna **111**(4-6): 168-173.

Jiao, H., M. Rutar, N. Fernando, T. Yednock, S. Sankaranarayanan, R. Aggio-Bruce, J. Provis and R. Natoli (2018). "Subretinal macrophages produce classical complement activator C1q leading to the progression of focal retinal degeneration." Molecular neurodegeneration **13**(1): 45.

Jung, M. K. and J. Y. Mun (2018). "Sample Preparation and Imaging of Exosomes by Transmission Electron Microscopy." Journal of visualized experiments : JoVE(131): 56482.

Kang, G.-Y., J. Y. Bang, A. J. Choi, J. Yoon, W.-C. Lee, S. Choi, S. Yoon, H. C. Kim, J.-H. Baek and H. S. Park (2014). "Exosomal proteins in the aqueous humor as novel biomarkers in patients with neovascular age-related macular degeneration." Journal of proteome research **13**(2): 581-595.

Kauppinen, A., J. J. Paterno, J. Blasiak, A. Salminen and K. Kaarniranta (2016). "Inflammation and its role in age-related macular degeneration." Cellular and molecular life sciences : CMLS **73**(9): 1765-1786.

Kim, S. R., N. Fishkin, J. Kong, K. Nakanishi, R. Allikmets and J. R. Sparrow (2004). "Rpe65 Leu450Met variant is associated with reduced levels of the retinal pigment epithelium lipofuscin fluorophores A2E and iso-A2E." Proceedings of the National Academy of Sciences of the United States of America **101**(32): 11668-11672.

Klingeborn, M., W. M. Dismuke, C. B. Rickman and W. D. Stamer (2017). "Roles of exosomes in the normal and diseased eye." Progress in retinal and eye research **59**: 158-177.

Knickelbein, J. E., C.-C. Chan, H. N. Sen, F. L. Ferris and R. B. Nussenblatt (2015). "Inflammatory mechanisms of age-related macular degeneration." International ophthalmology clinics **55**(3): 63.

Kosaka, N. (2010). "Secretory mechanisms and intercellular transfer of microRNAs in living cells." J Biol Chem **285**.

Kosaka, N., H. Iguchi, K. Hagiwara, Y. Yoshioka, F. Takeshita and T. Ochiya (2013). "Neutral sphingomyelinase 2 (nSMase2)-dependent exosomal transfer of angiogenic microRNAs regulate cancer cell metastasis." Journal of Biological Chemistry **288**(15): 10849-10859.

Kowal, J., M. Tkach and C. Théry (2014). "Biogenesis and secretion of exosomes." Current opinion in cell biology **29**: 116-125.

Krol, J., V. Busskamp, I. Markiewicz, M. B. Stadler, S. Ribi, J. Richter, J. Duebel, S. Bicker, H. J. Fehling, D. Schübeler, T. G. Oertner, G. Schratt, M. Bibel, B. Roska and W. Filipowicz (2010). "Characterizing Light-Regulated Retinal MicroRNAs Reveals Rapid Turnover as a Common Property of Neuronal MicroRNAs." Cell **141**(4): 618-631.

Kyosseva, S. V. (2016). "Targeting MAPK Signaling in Age-Related Macular Degeneration." Ophthalmology and eye diseases **8**: 23-30.

L Isola, A. and S. Chen (2017). "Exosomes: the messengers of health and disease." Current neuropharmacology **15**(1): 157-165.

Lachenal, G., K. Pernet-Gallay, M. Chivet, F. J. Hemming, A. Belly, G. Bodon, B. Blot, G. Haase, Y. Goldberg and R. Sadoul (2011). "Release of exosomes from differentiated neurons and its regulation by synaptic glutamatergic activity." Molecular and Cellular Neuroscience **46**(2): 409-418.

Lehmann, B. D., M. S. Paine, A. M. Brooks, J. A. McCubrey, R. H. Renegar, R. Wang and D. M. Terrian (2008). "Senescence-Associated Exosome Release from Human Prostate Cancer Cells." Cancer Research **68**(19): 7864.

Lener, T., M. Gimona, L. Aigner, V. Börger, E. Buzas, G. Camussi, N. Chaput, D. Chatterjee, F. A. Court and H. A. d. Portillo (2015). "Applying extracellular vesicles based therapeutics in clinical trials–an ISEV position paper." Journal of extracellular vesicles **4**(1): 30087.

Li, J. J., B. Wang, M. C. Kodali, C. Chen, E. Kim, B. J. Patters, L. Lan, S. Kumar, X. Wang and J. Yue (2018). "In vivo evidence for the contribution of peripheral circulating inflammatory exosomes to neuroinflammation." Journal of neuroinflammation **15**(1): 8.

Li, N., L. Zhao, Y. Wei, V. L. Ea, H. Nian and R. Wei (2019). "Recent advances of exosomes in immune-mediated eye diseases." Stem cell research & therapy **10**(1): 278.

Long, H., X. Wang, Y. Chen, L. Wang, M. Zhao and Q. Lu (2018). "Dysregulation of microRNAs in autoimmune diseases: Pathogenesis, biomarkers and potential therapeutic targets." Cancer letters **428**: 90-103.

Lu, Y.-Z., N. Fernando, R. Natoli, M. Madigan and K. Valter (2018). "670nm light treatment following retinal injury modulates Müller cell gliosis: Evidence from in vivo and in vitro stress models." Experimental eye research **169**: 1-12.

Luberto, C., D. F. Hassler, P. Signorelli, Y. Okamoto, H. Sawai, E. Boros, D. J. Hazen-Martin, L. M. Obeid, Y. A. Hannun and G. K. Smith (2002). "Inhibition of tumor necrosis factor-induced cell death in MCF7 by a novel inhibitor of neutral sphingomyelinase." J Biol Chem **277**(43): 41128-41139.

Mathieu, M., L. Martin-Jaular, G. Lavieu and C. Théry (2019). "Specificities of secretion and uptake of exosomes and other extracellular vesicles for cell-to-cell communication." Nature cell biology **21**(1): 9-17.

Mattapallil, M. J., E. F. Wawrousek, C.-C. Chan, H. Zhao, J. Roychoudhury, T. A. Ferguson and R. R. Caspi (2012). "The Rd8 mutation of the Crb1 gene is present in vendor lines of C57BL/6N mice and embryonic stem cells, and confounds ocular induced mutant phenotypes." Investigative ophthalmology & visual science **53**(6): 2921-2927.

Mead, B. and S. Tomarev (2020). "Extracellular vesicle therapy for retinal diseases." Progress in Retinal and Eye Research: 100849.

Natoli, R., N. Fernando, M. Madigan, J. A. Chu-Tan, K. Valter, J. Provis and M. Rutar (2017). "Microglia-derived IL-1β promotes chemokine expression by Müller cells and RPE in focal retinal degeneration." Molecular neurodegeneration **12**(1): 31.

Natoli, R., H. Jiao, N. L. Barnett, N. Fernando, K. Valter, J. M. Provis and M. Rutar (2016). "A model of progressive photo-oxidative degeneration and inflammation in the pigmented C57BL/6J mouse retina." Experimental eye research **147**: 114-127.

Natoli, R., Y. Zhu, K. Valter, S. Bisti, J. Eells and J. Stone (2010). "Gene and noncoding RNA regulation underlying photoreceptor protection: microarray study of dietary antioxidant saffron and photobiomodulation in rat retina." Molecular vision **16**: 1801.

Newman, A. M., N. B. Gallo, L. S. Hancox, N. J. Miller, C. M. Radeke and M. A. Maloney (2012). "Systems-level analysis of age-related macular degeneration reveals global biomarkers and phenotype-specific functional networks." Genome Med **4**.

Pascua-Maestro, R., E. González, C. Lillo, M. D. Ganfornina, J. M. Falcón-Pérez and D. Sanchez (2018). "Extracellular Vesicles Secreted by Astroglial Cells Transport Apolipoprotein D to Neurons and Mediate Neuronal Survival Upon Oxidative Stress." Front Cell Neurosci **12**: 526.

Piñero, J., À. Bravo, N. Queralt-Rosinach, A. Gutiérrez-Sacristán, J. Deu-Pons, E. Centeno, J. García-García, F. Sanz and L. I. Furlong (2016). "DisGeNET: a comprehensive platform integrating information on human disease-associated genes and variants." Nucleic Acids Research **45**(D1): D833-D839.

Ratnapriya, R. and A. Swaroop (2013). "Genetic architecture of retinal and macular degenerative diseases: the promise and challenges of next-generation sequencing." Genome medicine **5**(9): 84.

Rivera, J. C., M. Holm, D. Austeng, T. S. Morken, T. E. Zhou, A. Beaudry-Richard, E. M. Sierra, O. Dammann and S. Chemtob (2017). "Retinopathy of prematurity: inflammation, choroidal degeneration, and novel promising therapeutic strategies." Journal of neuroinflammation **14**(1): 165-165.

Robbins, P. D. and A. E. Morelli (2014). "Regulation of immune responses by extracellular vesicles." Nature Reviews Immunology **14**(3): 195-208.

Rübsam, A., S. Parikh and P. E. Fort (2018). "Role of Inflammation in Diabetic Retinopathy." International journal of molecular sciences **19**(4): 942.

Rupaimoole, R. and F. J. Slack (2017). "MicroRNA therapeutics: towards a new era for the management of cancer and other diseases." Nature Reviews Drug Discovery **16**: 203.

Rutar, M., R. Natoli, R. Chia, K. Valter and J. M. Provis (2015). "Chemokine-mediated inflammation in the degenerating retina is coordinated by Müller cells, activated microglia, and retinal pigment epithelium." Journal of neuroinflammation **12**(1): 8.

Rutar, M. V., R. C. Natoli and J. M. Provis (2012). "Small interfering RNA-mediated suppression of Ccl2 in Muller cells attenuates microglial recruitment and photoreceptor death following retinal degeneration." J Neuroinflammation **9**.

Sackmann, V., M. Sardar Sinha, C. Sackmann, L. Civitelli, J. Bergström, A. Ansell-Schultz and M. Hallbeck (2019). "Inhibition of nSMase2 reduces the transfer of oligomeric α-synuclein irrespective of hypoxia." Frontiers in molecular neuroscience **12**: 200.

Saeedi Borujeni, M. J., E. Esfandiary, G. Taheripak, P. Codoñer-Franch, E. Alonso-Iglesias and H. Mirzaei (2018). "Molecular aspects of diabetes mellitus: Resistin, microRNA, and exosome." Journal of cellular biochemistry **119**(2): 1257-1272.

Sarko, D. K. and C. E. McKinney (2017). "Exosomes: origins and therapeutic potential for neurodegenerative disease." Frontiers in neuroscience **11**: 82.

Skriner, K., K. Adolph, P. R. Jungblut and G. R. Burmester (2006). "Association of citrullinated proteins with synovial exosomes." Arthritis & Rheumatism: Official Journal of the American College of Rheumatology **54**(12): 3809-3814.

Slenter, D. N., M. Kutmon, K. Hanspers, A. Riutta, J. Windsor, N. Nunes, J. Mélius, E. Cirillo, S. L. Coort, D. Digles, F. Ehrhart, P. Giesbertz, M. Kalafati, M. Martens, R. Miller, K. Nishida, L. Rieswijk, A. Waagmeester, L. M. T. Eijssen, C. T. Evelo, A. R. Pico and E. L. Willighagen (2018). "WikiPathways: a multifaceted pathway database bridging metabolomics to other omics research." Nucleic acids research **46**(D1): D661-D667.

Słomka, A., S. K. Urban, V. Lukacs-Kornek, E. Żekanowska and M. Kornek (2018). "Large Extracellular Vesicles: Have We Found the Holy Grail of Inflammation?" Frontiers in Immunology **9**: 2723.

Soria, F. N., O. Pampliega, M. Bourdenx, W. G. Meissner, E. Bezard and B. Dehay (2017). "Exosomes, an Unmasked Culprit in Neurodegenerative Diseases." Frontiers in neuroscience **11**: 26-26.

Squadrito, M. L., C. Baer, F. Burdet, C. Maderna, G. D. Gilfillan, R. Lyle, M. Ibberson and M. De Palma (2014). "Endogenous RNAs modulate microRNA sorting to exosomes and transfer to acceptor cells." Cell reports **8**(5): 1432-1446.

Tam, S., M.-S. Tsao and J. D. McPherson (2015). "Optimization of miRNA-seq data preprocessing." Briefings in bioinformatics **16**(6): 950-963.

Team, R. C. (2019). "R: A Language and Environment for Statistical Computing." from http://www.R-project.org/.

Théry, C., L. Zitvogel and S. Amigorena (2002). "Exosomes: composition, biogenesis and function." Nature Reviews Immunology **2**(8): 569.

Van der Pol, E., A. N. Böing, P. Harrison, A. Sturk and R. Nieuwland (2012). "Classification, functions, and clinical relevance of extracellular vesicles." Pharmacological reviews **64**(3): 676-705.

Van Hezel, M. E., R. Nieuwland, R. Van Bruggen and N. P. Juffermans (2017). "The ability of extracellular vesicles to induce a pro-inflammatory host response." International journal of molecular sciences **18**(6): 1285.

Van Niel, G., I. Porto-Carreiro, S. Simoes and G. Raposo (2006). "Exosomes: a common pathway for a specialized function." Journal of biochemistry **140**(1): 13-21.

Vella, L. J., B. J. Scicluna, L. Cheng, E. G. Bawden, C. L. Masters, C.-S. Ang, N. Willamson, C. McLean, K. J. Barnham and A. F. Hill (2017). "A rigorous method to enrich for exosomes from brain tissue." Journal of extracellular vesicles **6**(1): 1348885-1348885.

Vidal-Gil, L., J. Sancho-Pelluz, E. Zrenner, M. Oltra and A. Sahaboglu (2019). "Poly ADP ribosylation and extracellular vesicle activity in rod photoreceptor degeneration." Scientific Reports **9**(1): 3758.

Wan, P., W. Su, Y. Zhang, Z. Li, C. Deng, J. Li, N. Jiang, S. Huang, E. Long and Y. Zhuo (2019). "LncRNA H19 initiates microglial pyroptosis and neuronal death in retinal ischemia/reperfusion injury." Cell Death & Differentiation: 1.

Wang, A. L., T. J. Lukas, M. Yuan, N. Du, M. O. Tso and A. H. Neufeld (2009). "Autophagy and exosomes in the aged retinal pigment epithelium: possible relevance to drusen formation and age-related macular degeneration." PloS one **4**(1): e4160.

Wang, K., H. Li, R. Sun, C. Liu, Y. Luo, S. Fu and Y. Ying (2018). "Emerging roles of transforming growth factor β signaling in wet age-related macular degeneration." Acta Biochimica et Biophysica Sinica **51**(1): 1-8.

Wickham, H. (2016). "ggplot2: Elegant Graphics for Data Analysis." Springer-Verlag New York.

Wong, W. Y., M. M. L. Lee, B. D. Chan, R. K. T. Kam, G. Zhang, A. P. Lu and W. C. S. Tai (2016). "Proteomic profiling of dextran sulfate sodium induced acute ulcerative colitis mice serum

exosomes and their immunomodulatory impact on macrophages." Proteomics **16**(7): 1131-1145.

Wooff, Y., S. M. Man, R. Natoli, R. Aggio-Bruce and N. Fernando (2019). "IL-1 Family members mediate cell death, inflammation and angiogenesis in retinal degenerative diseases." Frontiers in immunology **10**: 1618.

Wu, H., C. Wang and Z. Wu (2013). "A new shrinkage estimator for dispersion improves differential expression detection in RNA-seq data." Biostatistics (Oxford, England) **14**(2): 232-243.

Xiang, L., X.-J. Chen, K.-C. Wu, C.-J. Zhang, G.-H. Zhou, J.-N. Lv, L.-F. Sun, F.-F. Cheng, X.-B. Cai and Z.-B. Jin (2017). "miR-183/96 plays a pivotal regulatory role in mouse photoreceptor maturation and maintenance." Proceedings of the National Academy of Sciences **114**(24): 6376.

Xu, W., Y. Wu, Z. Hu, L. Sun, G. Dou, Z. Zhang, H. Wang, C. Guo and Y. Wang (2019). "Exosomes from Microglia Attenuate Photoreceptor Injury and Neovascularization in an Animal Model of Retinopathy of Prematurity." Molecular Therapy-Nucleic Acids **16**: 778-790.

Yáñez-Mó, M., P. R.-M. Siljander, Z. Andreu, A. Bedina Zavec, F. E. Borràs, E. I. Buzas, K. Buzas, E. Casal, F. Cappello and J. Carvalho (2015). "Biological properties of extracellular vesicles and their physiological functions." Journal of extracellular vesicles **4**(1): 27066.

Ye, S.-b., Z.-L. Li, D.-h. Luo, B.-j. Huang, Y.-S. Chen, X.-s. Zhang, J. Cui, Y.-x. Zeng and J. Li (2014). "Tumor-derived exosomes promote tumor progression and T-cell dysfunction through the regulation of enriched exosomal microRNAs in human nasopharyngeal carcinoma." Oncotarget **5**(14): 5439.

Yuana, Y., A. Sturk and R. Nieuwland (2013). "Extracellular vesicles in physiological and pathological conditions." Blood reviews **27**(1): 31-39.

Zhang, H.-G., C. Liu, K. Su, S. Yu, L. Zhang, S. Zhang, J. Wang, X. Cao, W. Grizzle and R. P. Kimberly (2006). "A membrane form of TNF-α presented by exosomes delays T cell activation-induced cell death." The Journal of Immunology **176**(12): 7385-7393.

Zhang, W., Y. Ma, Y. Zhang, J. Yang, G. He and S. Chen (2019). "Photo-Oxidative Blue-Light Stimulation in Retinal Pigment Epithelium Cells Promotes Exosome Secretion and Increases the Activity of the NLRP3 Inflammasome." Current eye research **44**(1): 67-75.

Zhao, Y., S. R. Weber, J. Lease, M. Russo, C. A. Siedlecki, L.-C. Xu, H. Chen, W. Wang, M. Ford and R. Simo (2018). "Liquid biopsy of vitreous reveals an abundant vesicle population

consistent with the size and morphology of exosomes." Translational vision science & technology **7**(3): 6-6.

Ziemann, M., A. Kaspi and A. El-Osta (2016). "Evaluation of microRNA alignment techniques." RNA (New York, N.Y.) **22**(8): 1120-1138.

Zuzic, M., J. E. Rojo Arias, S. G. Wohl and V. Busskamp (2019). "Retinal miRNA Functions in Health and Disease." Genes **10**(5): 377.